PLOS | PATHOGENS

RESEARCH ARTICLE

Identification of a Transcription Factor That Regulates Host Cell Exit and Virulence of *Mycobacterium tuberculosis*

Lalitha Srinivasan[1], Serdar A. Gurses[1¤], Benjamin E. Hurley[1], Jessica L. Miller[1], Petros C. Karakousis[2], Volker Briken[1]*

1 Department of Cell Biology and Molecular Genetics, University of Maryland, College Park, Maryland, United States of America, **2** Department of Medicine, Johns Hopkins University School of Medicine, Baltimore, Maryland, United States of America

¤ Current address: Department of Medical Biology, Emine-Bahaeddin Nakıboğlu School of Medicine, Zirve University, Gaziantep, Turkey
* vbriken@umd.edu

OPEN ACCESS

Citation: Srinivasan L, Gurses SA, Hurley BE, Miller JL, Karakousis PC, Briken V (2016) Identification of a Transcription Factor That Regulates Host Cell Exit and Virulence of *Mycobacterium tuberculosis*. PLoS Pathog 12(5): e1005652. doi:10.1371/journal.ppat.1005652

Editor: Christopher M. Sassetti, University of Massachusetts Medical School, UNITED STATES

Received: March 18, 2016

Accepted: May 1, 2016

Published: May 18, 2016

Data Availability Statement: All relevant data are within the paper and its Supporting Information files.

Funding: The research described was supported by National Institutes of Health/ National Institute of Allergy and Infectious Diseases grant R56 AI114269 to VB and R01AI083125 to PCK. The funders had no role in study design, data collection and analysis, decision to publish, or preparation of the manuscript.

Competing Interests: The authors have declared that no competing interests exist.

Abstract

The interaction of *Mycobacterium tuberculosis* (Mtb) with host cell death signaling pathways is characterized by an initial anti-apoptotic phase followed by a pro-necrotic phase to allow for host cell exit of the bacteria. The bacterial modulators regulating necrosis induction are poorly understood. Here we describe the identification of a transcriptional repressor, Rv3167c responsible for regulating the escape of Mtb from the phagosome. Increased cytosolic localization of Mtb*Δ*Rv3167c* was accompanied by elevated levels of mitochondrial reactive oxygen species and reduced activation of the protein kinase Akt, and these events were critical for the induction of host cell necrosis and macroautophagy. The increase in necrosis led to an increase in bacterial virulence as reflected in higher bacterial burden and reduced survival of mice infected with Mtb*Δ*Rv3167c*. The regulon of Rv3167c thus contains the bacterial mediators involved in escape from the phagosome and host cell necrosis induction, both of which are crucial steps in the intracellular lifecycle and virulence of Mtb.

Author Summary

Mycobacterium tuberculosis (Mtb), the causative agent of tuberculosis, is a highly successful human pathogen. Following entry into host phagocytic cells, Mtb resides within a modified phagosomal compartment and inhibits apoptotic host cell death. Recent studies have demonstrated that Mtb eventually translocates from the phagosomal compartment to the cytosol. This event is followed by the induction of necrotic host cell death allowing the bacteria to exit the host cell and infect naive cell populations. Our study adds to this relatively unexplored aspect of Mtb pathogenesis by revealing that the transcriptional repressor *Rv3167c* of Mtb negatively regulates phagosomal escape and host cell necrosis. We furthermore demonstrate that the increased necrosis induction by the Mtb mutant strain deficient in *Rv3167c* required elevated reactive oxygen species levels within host cell mitochondria

and reduced activation of the protein kinase Akt. In addition, the increased virulence of the Mtb mutant strain observed after aerosol infection of mice strengthens the link between the ability of the bacteria to induce host cell necrosis and virulence. The Mtb genes negatively regulated by Rv3167c are thus potential virulence factors that can be targeted for drug and vaccine development.

Introduction

Apoptosis is a major programmed cell death pathway but now it is well established that necrosis can also be induced via defined signal transduction pathways [1,2]. The importance of apoptosis in host defense against pathogens is well described [3,4]. In contrast, the function of programmed necrosis in host resistance or susceptibility to pathogens is still an open question in many cases and may depend upon the context of the infection and the pathogen [5]. For instance, the RIPK1/3 necrosis pathway acts as a back-up mechanism of death induction in cells infected with viruses that are able to inhibit host cell apoptosis [6]. Consequently, programmed necrosis is associated with increased host resistance against viral pathogens in the case of vaccinia virus, adenovirus and MCMV [5,6]. Nevertheless, for the influenza A virus, programmed necrosis leads to increased pathology and host susceptibility [7]. Limited results are available for interaction of bacterial pathogens with host cell necrosis pathways but similar to viral pathogens the role of programmed necrosis may vary depending upon the pathogen. Enteropathogenic *Escherichia coli* can inhibit RIPK3-dependent necrosis via the glycosyl transferase NleB and this activity is important for bacterial virulence [8,9]. In contrast, IRF-3-dependent necrosis induction by *Listeria monocytogenes* promotes pathogen dissemination and virulence [10].

The interaction of wild-type *Mycobacterium tuberculosis* (Mtb) with its host cell in regard to cell death signaling is complex [11–13]. According to one model, virulent strains of Mtb are capable of inhibiting host cell apoptosis during the early phase of the infection to allow for intracellular replication but the bacteria induce necrosis in order to exit the host cell at a later stage [14]. The discovery of *Mtb* genes that inhibit host cell apoptosis such as *nuoG* [15], *pknE* [16], *secA2* [17], *Rv3654c* [18], and *ndk* [19] supports this model. Furthermore, the Mtb *nuoG* mutant is attenuated in the mouse model of tuberculosis, thus illustrating the importance of host cell apoptosis inhibition for Mtb virulence [15]. Consistently, mice with reduced host cell apoptosis induction upon Mtb infection are more susceptible [20]. The mechanisms leading to increased host resistance include an increase in efferocytosis of apoptotic host cells leading to killing of the bacteria [21,22]. In addition, there are various lines of evidence that increased host cell apoptosis will lead to a more rapid and increased cytolytic T-cell response [17,23,24].

In contrast to apoptosis, host cell necrosis induction is associated with increased host susceptibility and virulence of Mtb as well as *Mycobacterium marinum* (Mm) in mice and in zebrafish [20,25]. Several studies demonstrated the central role of host cell eicosanoids lipoxin A_4 (LXA_4) and prostaglandin E_2 (PGE_2) in the regulation of host cell apoptosis versus necrosis induction and their importance for bacterial virulence and host resistance [24,26,27]. The enzyme Leukotriene A4 hydrolase (LTA4H) regulates synthesis of the eicosanoids LXA_4 and leukotriene B_4 (LTB_4); excessive production of either lipid mediator leads to macrophage necrosis [28]. Polymorphisms in LTA4H in humans are associated with hypersusceptibility to mycobacterial infections [29]. Lysosomal destabilization and macrophage necrosis was found to occur following accumulation of about 20 or more intracellular bacteria [30,31]. The escape of Mtb from the phagosome to the cytosol precedes necrosis and exit from the host cell [32–34]. The Mtb type

VII secretion systems, ESX-1 and ESX-5, are implicated in host cell necrosis induction. The deletion of the Mtb ESX-1 secretion system leads to a reduced induction of host cell necrosis and dissemination of the mutant mycobacteria [35–37], this could be due the inability of mutant strains to escape from the phagosome [33,34,38]. The Mtb ESX-5 system is involved in mediating cell necrosis after the bacteria have escaped the phagosome [39]. The PE25/PP41 complex secreted via ESX-5 may be one of the effectors of ESX-5-mediated host cell necrosis as addition of the purified protein complex induced necrosis of macrophages [40].

Host cell necrosis induction by Mtb is important for cell exit and dissemination but the molecular mechanisms involved are still poorly understood. Here we describe the discovery of a tetracycline repressor family protein, Rv3167c, which negatively regulates the capacity of the bacteria to induce host cell necrosis. Infection of macrophage with the *Rv3167c* deletion strain (Mtb*Δ*Rv3167c*) led to a rapid increase in host cell necrosis via a novel host cell signaling pathway that involves the reduced activation of the protein kinase Akt leading to an increase in mitochondrial reactive oxygen species (mROS). Interestingly, we discovered that Mtb*Δ*Rv3167c* escape the phagosome in higher numbers than wild-type Mtb, which most likely triggers the host cell necrosis signaling. Finally, aerosol infection of mice demonstrated the increased virulence of Mtb*Δ*Rv3167c*. In conclusion, we find that Rv3167c regulates the escape of Mtb from the phagosome, which marks the beginning of the host cell exit program of the Mtb intracellular life cycle.

Results

Rv3167c is important for inhibition of host cell programmed necrosis

We previously performed a gain-of-function genetic screen and identified a genomic region in Mtb H37Rv containing anti-apoptotic genes (S1A Fig) [15]. A series of deletion mutants spanning several genes within this region was generated and tested for loss of apoptosis inhibition. THP1 cells were infected with wild-type Mtb (Mtb) and the deletion mutants and stained for genomic DNA fragmentation using TUNEL assay. Two deletion mutants, one being the single gene *nuoG* mutant [15], and the other a five gene deletion mutant designated 7/10, induced higher levels of cell death compared to the Mtb control (S1B Fig). Screening of genes within the 7/10 region revealed that deletion of *Rv3167c* had the maximal effect on loss of cell death inhibition. Infection with the deletion mutant Mtb*Δ*Rv3167c* (Mtb*Δ*) resulted in almost a 3-fold increase in TUNEL-positive THP1 cells compared to infection with the control Mtb strain (S1C Fig). Both southern blotting and RT-PCR confirmed deletion of *Rv3167c* (S2A–S2C Fig). Increased cell death induction by Mtb*Δ*Rv3167c* was also observed in primary human monocyte derived macrophages (hMDMs) by hypodiploid staining which measures loss of genomic DNA content following cell death (Fig 1B). Cell death induction by the complement strain Mtb*Δ*Rv3167c*-C (Mtb*Δ*C) was comparable to Mtb (Fig 1A and 1B), thus confirming that *Rv3167c* is required for Mtb-mediated host cell death inhibition. Replication of Mtb*Δ* is similar to Mtb; both, in infected THP1 cells and in growth media (S2D and S2E Fig). Rv3167c is most likely a member of the tetracycline-like family of regulators (TFR) since 89% of the Rv3167c amino acid sequence can be modeled with 99.9% confidence to the highest scoring template, the TFR SCO0332 of *Streptomyces coelicolor*, using Phyre2 software.

Although TUNEL staining has been historically used for detection of apoptotic DNA fragmentation, recent studies have shown that necrotic cells can also be TUNEL positive [41–43]. A characteristic feature of apoptotic cells is preservation of cell membrane integrity [3]. To determine whether cell death induced by Mtb*Δ*Rv3167c* is accompanied by cell membrane damage, we tested for the presence of adenylate kinase, normally located within healthy cells, in the supernatants of THP1 cells using the Toxilight assay. At 24 and 48h, a 3-fold higher level

of adenylate kinase activity was detected in supernatant from MtbΔ*Rv3167c*-infected cells compared to uninfected controls (Fig 1C). Mtb-infected cells also undergo necrosis albeit at lower levels compared to MtbΔ*Rv3167c*-infected cells. Mtb has been previously shown to induce necrosis in a dose and time dependent manner and our data supports this observation [44]. It

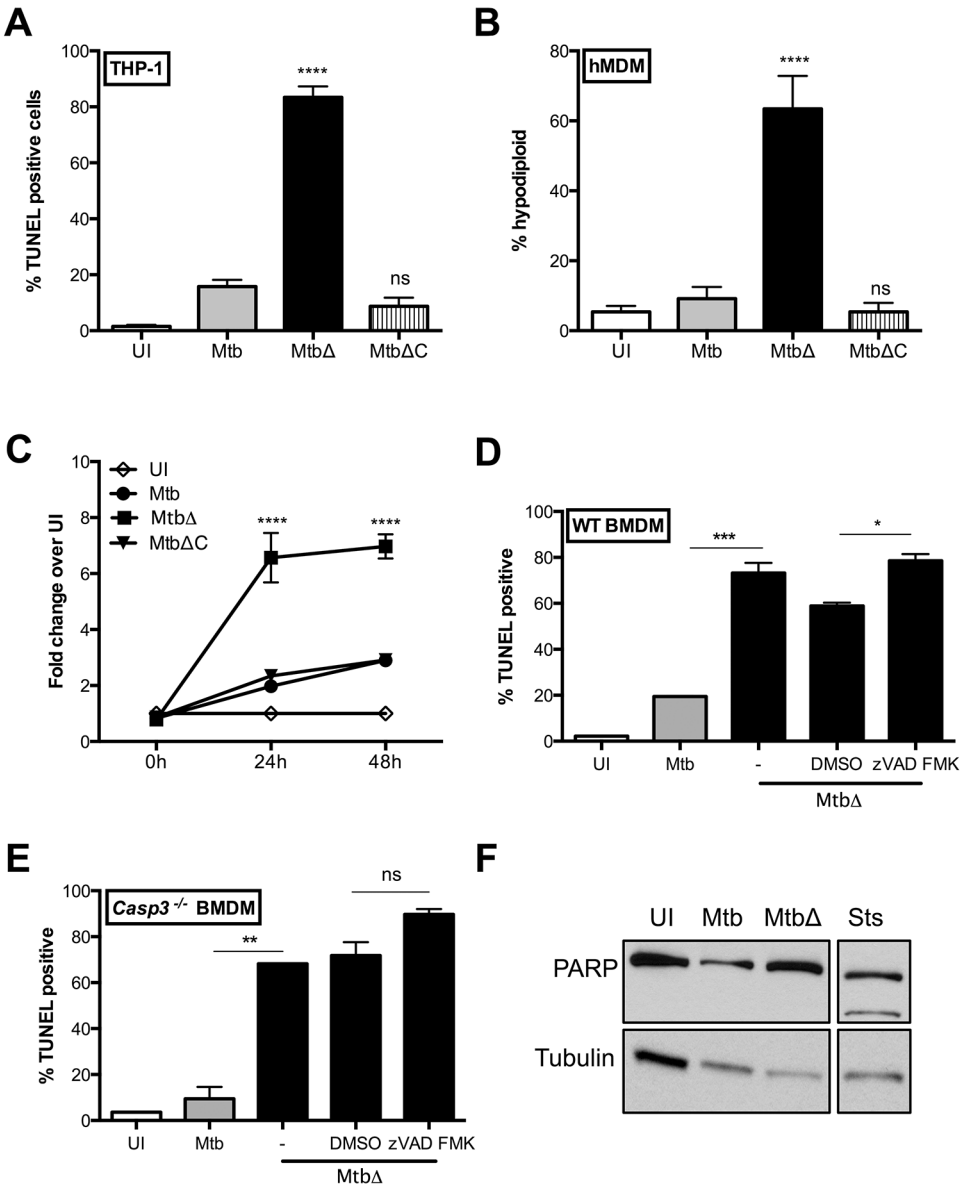

Fig 1. Mtb Rv3167c is important for inhibition of host cell death. Cell death induction in uninfected (UI), wild-type Mtb (Mtb), *Rv3167c* deletion mutant Mtb (MtbΔ) or complemented mutant Mtb (MtbΔC) bacteria infected cells was determined. (A) TUNEL staining and flow cytometry of THP1 cells at 24h (mean ± S.E.M, n = 6). (B) Cell death induction in human monocyte-derived macrophages (hMDMs) at 48h was measured by hypodiploid staining and flow cytometry. Cells were obtained from two independent donors (mean ± S.E.M, n = 6). (C) Release of adenylate kinase into supernatants from uninfected and infected THP1 cells was measured by Toxilight assay at the indicated time points (mean ± S.E.M, n = 6). Cell death induction in (D) wild type (WT) and (E) *Casp3*$^{-/-}$ BMDMs was determined by TUNEL staining and flow cytometry at 24h. Cells were treated with the pan caspase inhibitor zVAD-fmk (40μM) for one hour prior to and throughout the infection (mean ± S.E.M, n = 3). (F) PARP cleavage in THP1 cells at 24h detected by western blotting of whole cell lysates obtained from infected cells or after treatment with apoptosis inducer staurosporine (Sts). Image is representative of three independent experiments.

doi:10.1371/journal.ppat.1005652.g001

is important to note that the Toxilight assay cannot differentiate between primary necrosis or secondary necrosis of apoptotic cells and consequently further analysis into the nature of the induced cell death was required.

Execution of apoptotic cell death requires the cleavage and activation of the effector caspases-3, -6 and -7 [2]. We infected wild type (WT) and *Casp3*$^{-/-}$ bone marrow derived macrophages (BMDMs) and performed TUNEL staining to confirm that Mtb*Δ*Rv3167c* does not induce apoptotic cell death. No differences in TUNEL-positive cells were observed between Mtb*Δ*Rv3167c*-infected WT and *Casp3*$^{-/-}$ BMDMs (Fig 1D and 1E). To ensure that the lack of death inhibition in *Casp3*$^{-/-}$ BMDMs is not due to redundancy of caspase-3 with other effector caspases, the pan-caspase inhibitor zVAD-FMK was added to Mtb*Δ*Rv3167c*-infected cells. Inclusion of zVAD-FMK did not inhibit Mtb*Δ*Rv3167c*-induced cell death in both WT and *Casp3*$^{-/-}$ BMDMs (Fig 1E) although it did inhibit apoptosis induced by camptothecin (S3A Fig). We also did not observe cleavage of the DNA repair enzyme PARP, another feature of apoptosis, in Mtb or Mtb*Δ*Rv3167c*-infected THP1 cells (Fig 1F). Furthermore, the zVAD-FMK inhibitor was added to infected *Ripk3*$^{-/-}$ cells and had no effect on Mtb*Δ*Rv3167c*-induced cell death (S3D Fig). These results show that *Rv3167c* is required for inhibition of Mtb-induced necrotic host cell death.

Mtb*Δ*Rv3167c*-mediated cell death involves lysosomal membrane permeabilization

Next, we investigated the involvement of programmed necrosis pathways in cell death mediated by Mtb*Δ*Rv3167c*. In conditions where caspase-8 expression and activation are inhibited, the serine threonine protein kinases RIPK1 and RIPK3 induce necrosis downstream of TNF-receptor ligation via increased reactive oxygen species (ROS) generation, mitochondrial fission and formation of plasma membrane pores [45–48]. RIPK1 and RIPK3 have also been implicated in TNF-mediated necrosis in Mm-infected zebrafish [49]. We investigated the involvement of RIPK1 and RIPK3 in Mtb*Δ*Rv3167c*-induced cell death by using *Ripk3*$^{-/-}$ BMDM's and the RIPK1 inhibitor necrostatin1 (Nec1). Similar levels of PI-positive cells were observed in Mtb*Δ*Rv3167c*-infected *Ripk3*$^{-/-}$ BMDMs and Nec1 treated cells compared to WT BMDMs and solvent control-treated cells respectively (Figs 2A and S3B). Nec1 efficacy was confirmed by its ability to inhibit LPS and zVAD FMK induced RIPKI dependent cell death (S3C Fig) [50]. Necrosis induction following TNF treatment has been reported to change to apoptosis in the absence of RIPK1 and consequently, the absence of an effect on cell death induction by Mtb*Δ*Rv3167c* could be due to an increase in apoptosis in cells deficient in RIPK1/3 signaling [1]. Addition of zVAD-FMK to *Ripk3*$^{-/-}$ cells did not affect Mtb*Δ*Rv3167c*-induced cell death thereby ruling out a switch between apoptosis and necrosis in Mtb*Δ*Rv3167c*-infected cells (S3D Fig). Infection of *Tnfr1*$^{-/-}$ BMDMs established that Mtb*Δ*Rv3167c*-induced necrosis was independent of TNF signaling (S4A Fig). The DNA repair enzyme PARP1 has been implicated in necrosis induction via ATP depletion and nuclear translocation of mitochondrial apoptosis inducing factor in response to DNA alkylating agents and infection with BCG and enterovirus71 [51–53]. Necrosis induction by Mtb*Δ*Rv3167c* is independent of PARP1 since similar levels of necrosis were observed in infected *Parp1*$^{-/-}$ BMDMs and WT control cells (Fig 2B). The pro-inflammatory caspases, caspase-1 and caspase-11 have been shown to be involved in necrosis induction in response to several bacterial pathogens [54,55]. The role of these caspases in Mtb*Δ*Rv3167c*-induced necrosis was excluded by PI staining of *Casp1/11*$^{-/-}$ BMDMs (Fig 2C). NLRP3-dependent but caspase-1-independent necrosis has been reported to occur in response to infection with Mtb and *Shigella flexneri* [56,57]. Using immortalized NLRP3-deficient BMDMs we ruled out involvement of NLRP3 in Mtb*Δ*Rv3167c*-induced necrosis (S4C Fig).

Silencing of the inflammasome component ASC did not inhibit Mtb*Δ*Rv3167c*-induced necrosis as measured by the toxilight assay, rather necrosis was increased in Mtb*Δ*Rv3167c*-infected THP1shASC cells compared to control cells (S4D Fig). Involvement of IFNβ signaling (S4E and S4F Fig) and TLR signaling (S5A–S5C Fig) was also ruled out in necrosis induction by Mtb*Δ*Rv3167c*. These data indicate that Mtb*Δ*Rv3167c* does not engage the pathways of programmed necrosis currently described in the literature to induce host cell death.

Lysosomal membrane permeabilization (LMP) and the subsequent release of lysosomal contents into the cell cytosol leads to cell death [58,59]. Moderate lysosomal permeabilization leads to apoptosis while more severe damage precedes necrosis [60]. Lysosomal permeabilization and cathepsin release into the cytosol has been previously observed in cells infected with Mtb at high MOI [61]. To investigate whether LMP contributes to Mtb*Δ*Rv3167c*-induced cell death, we used the dye acridine orange (AO) that accumulates within lysosomes. A two-fold increase in the number of cells with loss of AO staining was observed as early as 8h post infection in Mtb*Δ*Rv3167c*-infected THP1 cells compared to Mtb-infected controls (Fig 2D). After 20h of infection the difference was even more pronounced with only about 8% of Mtb-infected cells showing low AO-staining compared to about 25% in mutant infected cells (Fig 2D). This indicates that LMP precedes necrosis induction by Mtb*Δ*Rv3167c* and is not merely a consequence of the disintegration of the cell triggered via a different mechanism.

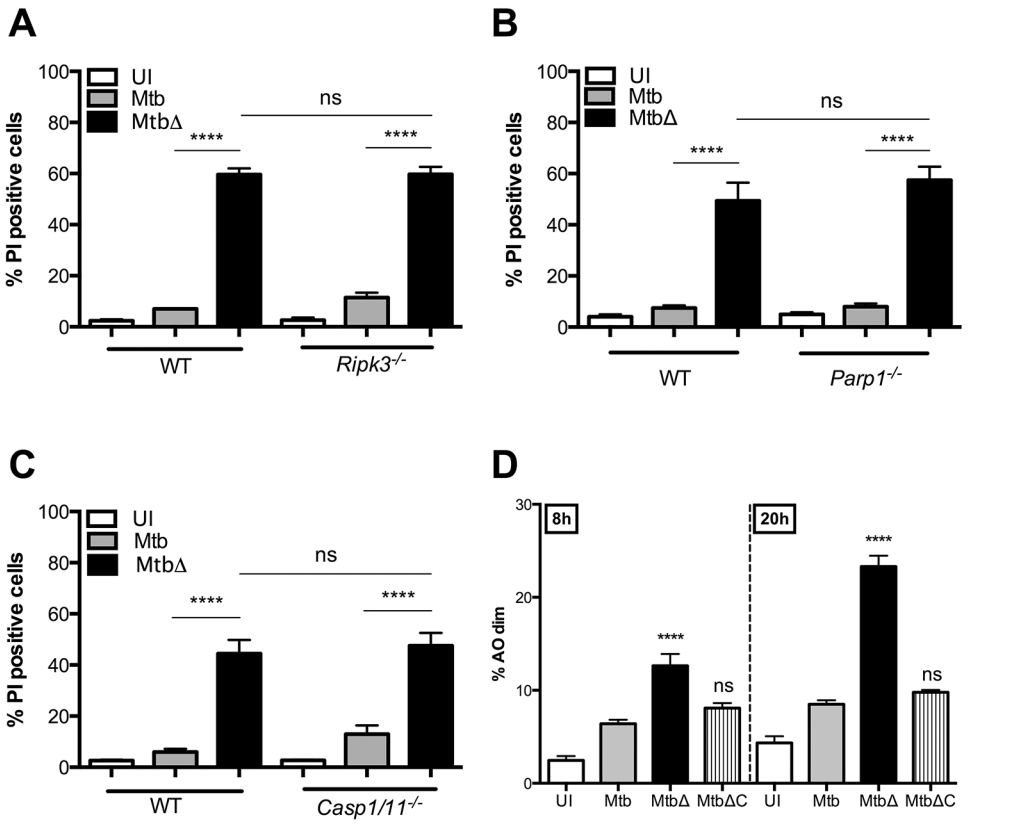

Fig 2. Mtb*Δ*Rv3167c* mediates cell death via programmed necrosis. (A) Necrosis induction in WT and *Ripk3*$^{-/-}$ BMDMs was measured by PI staining and flow cytometry at 24h (mean ± S.E.M, n = 3) in uninfected (UI), wild-type Mtb (Mtb), *Rv3167c* deletion mutant Mtb (MtbΔ) or complemented mutant Mtb (MtbΔC) bacteria infected cells. (B) Necrosis induction in WT and *Parp1*$^{-/-}$ BMDMs at 72h was determined by PI staining (mean ± S.E.M, n = 3). (C) Necrosis induction in WT and *Casp1/11*$^{-/-}$ BMDMs was determined by PI staining at 48h (mean ± S.E.M, n = 6). (D) Increases in lysosomal permeabilization were measured by acridine orange staining at indicated time points (mean ± S.E.M, n = 6).

doi:10.1371/journal.ppat.1005652.g002

Mtb Δ*Rv3167c* causes increased macroautophagy but not autophagic cell death

Autophagy is a catabolic process that allows for cell survival via recycling of cellular contents and contributes to pathogen elimination [62]. However, autophagy induction can also lead to cell death [63]. Therefore, we investigated whether Mtb Δ*Rv3167c* could induce autophagy in macrophages. First, we analyzed recruitment of LC3 into aggregates, an indicator of autophagy, by confocal microscopy [64]. THP1 cells expressing GFP-tagged LC3 (THP1 LC3GFP) were infected with AF647-NHS stained bacteria and at 8h, the percentage of cells showing aggregation of LC3 was estimated. A two-fold increase in autophagosome formation was observed in Mtb Δ*Rv3167c*-infected cells compared to Mtb-infected control cells (Fig 3A). Previous studies have shown that Mtb induces xenophagy resulting in co-localization of bacteria with autophagosomes and bacterial killing [65,66] However, we observed minimal colocalization of both Mtb and Mtb Δ*Rv3167c* (<1%) with autophagosomes (Fig 3A). This was confirmed by examination of infected THP1 cells by transmission electron microscopy (TEM) (Fig 3B). Next, we measured conversion of cytosolic LC3I to autophagosomal membrane bound LC3II, another hallmark of autophagy [64]. Uninfected and infected THP1 LC3GFP cells were washed with saponin-containing buffer leading to removal of cytosolic LC3I-GFP. Retention of autophagosomal membrane-bound LC3II-GFP was examined by flow cytometry [67]. A two-fold increase in autophagy induction was observed in Mtb Δ*Rv3167c*-infected cells compared to those infected with Mtb and Mtb Δ*Rv3167c*-C (Fig 3C). Increased conversion of both GFP tagged and endogenous LC3I to LC3II in Mtb Δ*Rv3167c*-infected cells was also seen by immunoblotting (Fig 3D). Autophagy induction by Mtb Δ*Rv3167c* was confirmed using 3-methyladenine (3-MA), a classical autophagy inhibitor [64]. Inclusion of 3-MA inhibited LC3II formation by Mtb Δ*Rv3167c* in THP1 LC3GFP cells (Fig 3E).

Increased accumulation of LC3II can be attributed either to an increase in autophagosome formation or to a decrease in LC3II degradation due to inhibition of autophagosome-lysosome fusion and maturation [64]. Addition of the vacuolar H^+ ATPase inhibitor bafilomycin A1 (BafA1) that inhibits autophagosomal degradation to Mtb Δ*Rv3167c*-infected THP1 LC3GFP cells led to a further increase in LC3II levels (S6A Fig). Autophagosome maturation leads to the degradation of LC3GFP to yield free GFP [64]. GFP was detected only in Mtb Δ*Rv3167c*-infected cells by immunoblotting (S6B Fig). These data indicate that Mtb Δ*Rv3167c*-induced autophagy but did not inhibit the maturation of the autophagosome. Finally to determine whether necrotic death of Mtb Δ*Rv3167c*-infected cells was a consequence of autophagy induction, we measured adenylate kinase release from $Atg5^{fl/fl}$ LysM Cre^+ ($Atg5^{-/-}$) and $Atg5^{fl/fl}$ LysM Cre^- ($Atg5^{+/+}$) BMDMs. We observed no differences in necrosis induction by Mtb Δ*Rv3167c* in autophagy-deficient $Atg5^{-/-}$ cells compared to the $Atg5^{+/+}$ controls (Fig 3F). Additionally, the inclusion of 3-MA did not result in inhibition of Mtb Δ*Rv3167c*-induced cell death in THP1 cells (S6C Fig). Therefore, while Mtb Δ*Rv3167c*-infected cells undergo macroautophagy, this does not contribute to their death via necrosis.

Rv3167c regulates escape of Mtb from the phagosome

The concept that Mtb resides within phagosomal compartments at all times has been challenged by recent studies demonstrating bacillary escape to the cytosol both *ex vivo* and *in vivo* [32–34,38]. Necrosis induction by Mtb and Mm was shown to closely follow escape to the cytosol [33,68]. We examined cytosolic escape by Mtb Δ*Rv3167c* using a fluorescence resonance energy transfer (FRET) based assay [33,34,69]. Uninfected and infected THP1 cells differentiated for three days with PMA were loaded with CCF4-AM. Intact CCF4-AM emits green fluorescence (535nm) due to FRET between the fluorescent moieties. Cleavage of CCF4-AM by β-lactamase

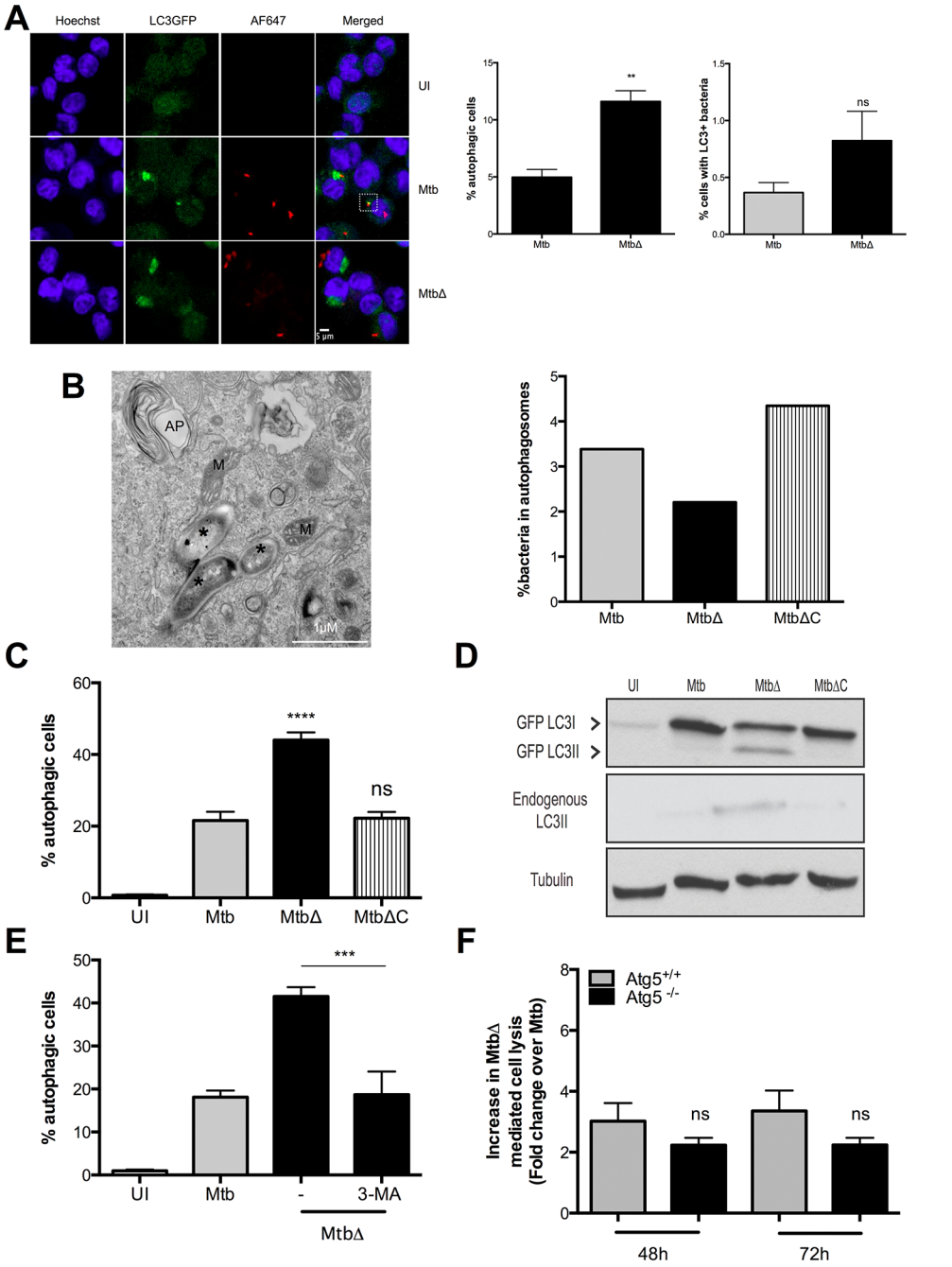

Fig 3. MtbΔ*Rv3167c* causes increased macroautophagy but not autophagic cell death. Uninfected (UI), wild-type Mtb (Mtb), *Rv3167c* deletion mutant Mtb (MtbΔ) or complemented mutant Mtb (MtbΔC) bacteria infected cells were analyzed as described. (A) Autophagy induction by AF647-NHS ester stained bacteria in THP1 LC3GFP cells at 8h examined by confocal microscopy. *Left*: Representative fluorescent image. The white box indicates bacteria colocalizing with LC3GFP. *Right*: Quantitative analysis of autophagic cells and cells with LC3+ bacteria. At least 450 cells were counted per condition per experiment. Statistical analysis was performed using unpaired Student's t test (mean ± S.E.M, n = 3). (B) *Left*: Representative TEM image showing absence of colocalization between bacteria and autophagosomes at 24h. *—bacteria; AP—autophagosome; M—mitochondria. *Right*: Quantitative analysis of bacteria within autophagosomes as observed by TEM. Atleast 10 cells were counted per condition per experiment (n = 2). (C) Autophagy induction in THP1 LC3GFP cells measured at 16h by flowcytometry (mean ± S.E.M, n = 6). (D) Conversion of GFP tagged and endogenous LC3I to LC3II detected by western blotting in whole cell lysates. Image is representative of three independent experiments. (E) Inhibition of MtbΔ*Rv3167c*-induced autophagy in

presence of 3-MA (5mM) measured by flowcytometry at 16h (mean ± S.E.M, n = 4). (F) Necrosis induction in autophagy competent ($Atg5^{+/+}$) and autophagy deficient ($Atg5^{-/-}$) BMDMs measured using Toxilight assay (mean ± S.E.M, n = 6).

doi:10.1371/journal.ppat.1005652.g003

expressed by cytosolic bacteria leads to FRET loss and a shift in the emission wavelength to 450nm that was measured by flow cytometry. Cells were co-stained with Live/Dead Fixable Red stain to restrict analysis to live cells only. While minor increases in fluorescence emission at 450nm were observed in Mtb-infected cells compared to uninfected cells at 48h, the largest shift in the CCF4 emission spectrum was seen in Mtb*Δ*Rv3167c*-infected cells (Fig 4A and 4B). A three-fold increase was observed in MFI_{450nm} of cells infected with Mtb*Δ*Rv3167c* compared to Mtb-infected controls. Increased cytosolic escape of Mtb*Δ*Rv3167c* was reversed following complementation (Fig 4A–4C). The pro-necrotic phenotype of Mtb*Δ*Rv3167c* was preserved in these macrophages (Fig 4D). Bacterial β-lactamase activity was not affected by either deletion of *Rv3167c* or gene complementation (S7 Fig).

To confirm the increased cytosolic escape by Mtb*Δ*Rv3167c*, we examined infected THP1 cells by TEM and quantified cytosolic bacteria in a double-blinded fashion by examining for absence of phagosomal membranes in healthy cells (Fig 4E, *above*). Increased presence of Mtb*Δ*Rv3167c* was observed in the cytosol at 8h compared to controls although statistical significance was not achieved. At 24h, 60% of Mtb*Δ*Rv3167c* were found to be cytosolic compared to 20% of Mtb corroborating the increased cytosolic escape by Mtb*Δ*Rv3167c* observed with the CCF4-AM assay (Fig 4E, *below*). A reduction of cytosolic escape was observed in cells infected with the complemented *MtbΔRv3167c*-C strain (Fig 4E, *below*). These data suggest that Rv3167c negatively regulates Mtb escape from the phagosome to the cytosol, an event that has been shown to be followed by induction of host cell necrosis [33,34].

Host kinase Akt1/2 is central to autophagy and necrosis induction by Mtb*Δ*Rv3167c*

Next we investigated the molecular mechanisms underlying autophagy induction by Mtb*Δ*Rv3167c*. The mitogen activated protein kinases (MAPKs) JNK and p38 have been implicated in autophagic responses of cells infected with Mtb following exposure to cytokines and vitamin D3 [70,71]. Mtb Eis has been shown to inhibit autophagy induction by suppressing JNK activation [72]. Hence we examined MAPK activation in response to Mtb*Δ*Rv3167c* infection by immunoblotting for phosphorylated forms in whole cell lysates prepared from infected THP1 LC3GFP cells at the indicated times. JNK activation was not observed at 0h, however increased JNK phosphorylation was detected in Mtb*Δ*Rv3167c*-infected cells compared to those infected with Mtb and Mtb*Δ*Rv3167c*-C at 18h (Fig 5A). In contrast to JNK, increased p38MAPK activation was observed in Mtb*Δ*Rv3167c*-infected cells at 0h. However by 18h, p38MAPK phosphorylation in Mtb*Δ*Rv3167c*-infected cells was similar to control cells infected with Mtb and Mtb*Δ*Rv3167c*-C (Fig 5A). Consistent results were observed in human monocyte-derived macrophages (hMDMs) as well; however, elevated JNK activation could be detected earlier at 0h in Mtb*Δ*Rv3167c*-infected cells (Fig 5B). We then determined whether JNK and p38MAPK contributed to autophagy induction by Mtb*Δ*Rv3167c*. THP1 LC3GFP cells were pre-treated and infected with JNK (SP600125) or p38MAPK (SB203580) inhibitors prior to infection with Mtb*Δ*Rv3167c*; the percentage of autophagic cells was measured by flow cytometry. Inclusion of the JNK inhibitor led to a partial, dose-dependent decrease in autophagy induction by Mtb*Δ*Rv3167c* while the p38MAPK inhibitor exerted no effects (Fig 5C). Neither of the inhibitors reversed the pro-necrotic phenotype of Mtb*Δ*Rv3167c*, instead a modest increase in PI-positive cells was observed in both cases (Fig 5D and 5E).

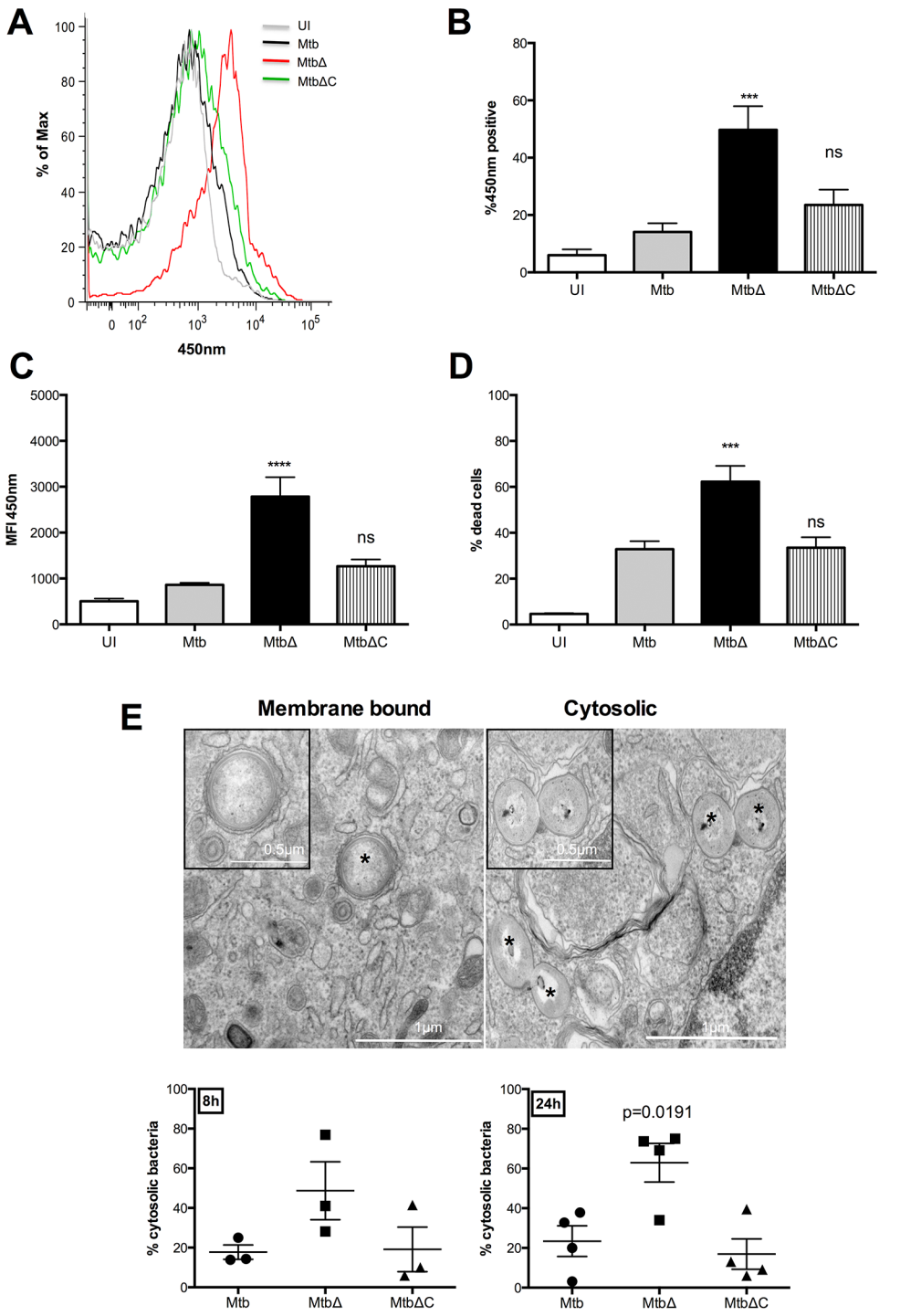

Fig 4. Rv3167c regulates escape of Mtb from the phagosome. Uninfected (UI), wild-type Mtb (Mtb), *Rv3167c* deletion mutant Mtb (MtbΔ) or complemented mutant Mtb (MtbΔC) bacteria infected cells were analyzed as described. CCF4 FRET-based flow cytometry was performed in combination with Live-Dead cell viability assays to examine phagosomal escape. Cells were gated to exclude dead populations and subsequent analysis was performed on live cells only. (A) Representative histograms demonstrating increased loss of FRET at 48h (corresponding to increased MFI_{450nm}) in MtbΔ-infected THP1 cells compared to Mtb- and MtbΔC-infected cells. (B) and (C) Quantification of (A) (mean ± S.E.M, n = 6). (D) Cell death induction measured by Live-Dead cell viability assay (mean ± S.E.M, n = 6). (E) *Above*: Representative TEM image of membrane bound and cytosolic mycobacteria within THP1 cells. *—bacteria. Inset: Magnified

images of bacteria. *Below*: Quantitative analysis of cytosolic bacteria as observed by TEM at 8h and 24h. At least 10 cells were counted per condition per experiment (mean ± S.E.M, n = 3).

doi:10.1371/journal.ppat.1005652.g004

The serine threonine protein kinase Akt functions as a critical negative regulator of autophagy at the initiation stage by activating mTOR and at the nucleation step by phosphorylating Beclin1 [73,74]. Inhibition of Akt activation has been implicated both in macroautophagy induction in response to nutritional stresses as well as selective autophagy-induction in response to pathogens such as *Toxoplasma gondii* and *Salmonella typhimurium* [73,75,76]. To determine role of Akt in autophagy-induction by MtbΔ*Rv3167c*, we examined Akt phosphorylation by immunoblotting. A complete loss of Akt activation was observed in MtbΔ*Rv3167c*-infected cells compared to the controls (Fig 5F). Consistently, the Akt activator, sc-79, inhibited autophagy induction by MtbΔ*Rv3167c* in a dose-dependent manner (Fig 5G) [77]. Additionally, Akt inhibition exerts effects on MtbΔ*Rv3167c*-mediated necrosis as well, since sc-79 significantly reduced MtbΔ*Rv3167c*-induced necrotic cell death (Fig 5H).

Mitochondrial ROS is required for cell death and autophagy induction by MtbΔ*Rv3167c*

Mtb-mediated suppression of reactive oxygen species (ROS) generated by the host phagocytic NADPH oxidase complex (NOX2) has been shown to inhibit host cell apoptosis [78]. Conversely, necrosis-induction by Mm has been shown to require mitochondrial ROS generation [49]. To determine whether necrosis-induction by MtbΔ*Rv3167c* involves ROS, we first measured ROS levels in cells infected by MtbΔ*Rv3167c*. Uninfected and infected BMDMs were stained with the either 2'7'-dichlorofluorescein diacetate (DCFDA) or MitoSOX Red for measurement of cytosolic and mitochondrial ROS respectively. At 0h, similar levels of ROS were observed in all infected cells compared to the uninfected controls (Fig 6A and 6B). However by 24h, approximately three-fold higher levels of both cytosolic and mitochondrial ROS were detected in MtbΔ*Rv3167c*-infected cells compared to those infected with Mtb and MtbΔ*Rv3167c*-C (Fig 6A and 6B). Next we examined whether increased ROS levels contribute to necrosis induction by MtbΔ*Rv3167c* using the flavoprotein inhibitor diphenylene iodonium (DPI) and the ROS scavengers glutathione and N-acetyl cysteine (NAC). Inclusion of these inhibitors and scavengers reversed necrosis induction by MtbΔ*Rv3167c* to levels observed in uninfected cells (S8A and S8B Fig). Thus, elevated ROS levels in MtbΔ*Rv3167c*-infected cells contribute to their necrotic cell death. Furthermore, addition of DPI to MtbΔ*Rv3167c*-infected THP1 LC3GFP cells completely abrogated autophagy induction compared to control cells (S8C Fig).

As ROS in eukaryotic cells may be derived from the NOX2 complex or mitochondria, we sought to determine which of these sources is implicated in necrosis-induction by MtbΔ*Rv3167c*. Similar levels of necrosis induction by MtbΔ*Rv3167c* were detected in WT and *Nox2*$^{-/-}$ BMDMs by PI staining (Fig 6C). However, a complete inhibition of MtbΔ*Rv3167c*-mediated cell death was observed in mCAT BMDMs obtained from transgenic mice overexpressing mitochondrial targeted human catalase (Fig 6D). Increased mitochondrial ROS generation was also accompanied by a time dependent loss of mitochondrial membrane potential as measured by $DIOC_6$ staining of MtbΔ*Rv3167c*-infected cells (S8D Fig). Increased mROS generation in MtbΔRv3167c-infected cells was found to be attributable to reduced Akt activation as inclusion of the Akt activator sc-79 inhibited mROS generation (Fig 6E). Taken together, our data reveal Akt and mitochondrial ROS to be critical regulators of MtbΔ*Rv3167c*-mediated necrosis and autophagy.

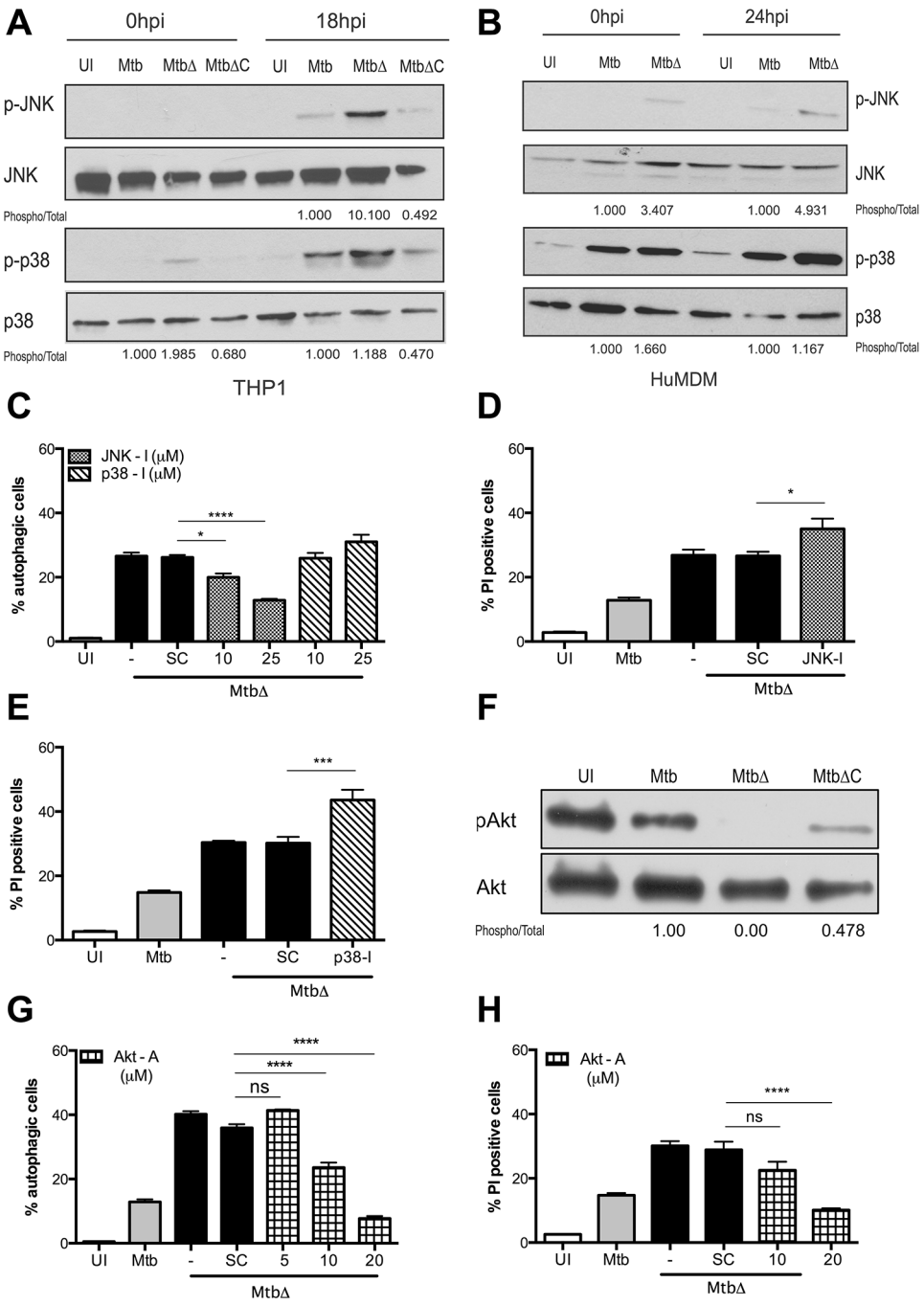

Fig 5. Host kinase Akt1/2 regulates MtbΔ*Rv3167c*-mediated autophagy and necrosis signaling. Uninfected (UI), wild-type Mtb (Mtb), *Rv3167c* deletion mutant Mtb (MtbΔ) or complemented mutant Mtb (MtbΔC) bacteria infected cells were analyzed as described. (A) JNK and p38 MAPK phosphorylation in THP1 LC3GFP cells at 18h detected by western blotting of whole cell lysates. Image is representative of three independent experiments. (B) JNK and p38 MAPK phosphorylation in human monocyte derived macrophages (hMDMs) at 24h detected by western blotting of whole cell lysates. Image is representative of three independent experiments. Cells were obtained from two donors. (C) Autophagy induction in presence of JNK (JNK-I—SP600125) and p38 MAPK (p38-I-SB203580) inhibitors detected by flow cytometry (mean ± S.E.M, n = 6). (D) Effect of JNK inhibitor (JNK-I-SP600125, 25μM) and (E) p38MAPK inhibitor (p38-I-SB203580, 25μM) on necrosis measured by PI staining and flow cytometry at 24h (mean ± S.E.M, n = 6). (F) Akt phosphorylation in THP1 LC3GFP cells detected at 16h by western blotting. Image is representative of three independent experiments. (G) Autophagy induction in presence of Akt activator (Akt—

A—sc-79) examined by flow cytometry at 16h (mean ± S.E.M, n = 8). (H) Necrosis induction in presence of Akt activator (Akt—A—sc-79) in THP1 macrophages measured by flow cytometry at 24h (means ± S.E.M, n = 6). For immunoblots, numbers below indicate fold change in band intensity compared to Mtb sample after normalization to loading control.

doi:10.1371/journal.ppat.1005652.g005

Rv3167c regulates virulence of Mtb

We assessed the contribution of *Rv3167c* to Mtb virulence *in vivo* by performing a survival study of C57Bl/6 mice infected with approximately 100 CFU of Mtb, Mtb*Δ*Rv3167c* and Mtb*Δ*Rv3167c*-C via the aerosol route. Increased mortality was observed in Mtb*Δ*Rv3167c*-infected mice (median survival time—33 weeks) compared to those infected with Mtb or Mtb*Δ*Rv3167c*-C (median survival times– 59 and 60 weeks respectively) (Fig 7A). Decreased survival following Mtb*Δ*Rv3167c* infection was also observed in immunodeficient SCID mice (S9A Fig). Lung bacterial burden on day one after infection was similar for all three strains indicating comparable initial inoculum of infection in both C57Bl/6 and SCID mice (Figs 7B and S9B). Relative to control mice, the lung bacillary burden was 10-fold higher in Mtb*Δ*Rv3167c*-infected animals at14 and 28 days, and this difference was magnified by day 56 following aerosol infection (Fig 7B). Increased bacterial burdens also were observed in the liver and spleen of Mtb*Δ*Rv3167c*-infected mice relative to control mice (Fig 7C and 7D). Higher levels of pro-inflammatory cytokines (TNF, IL1α and IL6) (Fig 7E) and chemokines (CCL3, CCL5 and MMP9) (Fig 7F) were detected in the lung tissues of mice infected with Mtb*Δ*Rv3167c*. Comparison of lung histopathology revealed a two-fold increase in cellular infiltration in Mtb*Δ*Rv3167c*-infected animals (Fig 7G).

Consistent with the findings in the mouse model of chronic TB infection, increased bacterial burdens were observed in the lungs of guinea pigs infected with *MtbΔRv3167c* relative to controls at 28 days following aerosol infection with similar bacterial loads (S9C and S9D Fig). Mtb*Δ*Rv3167c* was also found to induce cell death in *ex vivo* infection of guinea pig alveolar macrophages by TUNEL staining (S9E Fig). Collectively, these results show that Rv3167c negatively regulates Mtb virulence.

Discussion

The intracellular location of bacteria has important consequences for their recognition by the host and the generation of innate and adaptive immune responses. Mtb was thought to restrict itself to a modified host cell phagosomal compartment after infection [79,80]. However, electron microscopy studies performed on infected macrophages and dendritic cells provided evidence that Mtb and other mycobacterial species are present in the cytosol and that phagosomal escape is dependent upon the ESX-1 secretion system [32,38]. This was confirmed by a FRET-based method dependent on β-lactamase production by Mtb in *ex vivo*-infected cells as well as in pulmonary phagocytic cells obtained from infected mice [33,34]. We report in the current study that the mycobacterial gene *Rv3167c* negatively regulates the escape of Mtb from the phagosome to the cytosol (Fig 4). Our study is the first to suggest that Mtb can exert temporal control on phagosomal escape as Mtb*Δ*Rv3167c* was found in the cytosol as early as 24h after infection while Mtb has been reported to access the cytosol much later in the infection process (4–5 days) [33]. We hypothesize that *Rv3167c* represses cytosolic escape at early stages when the bacterial load is low, favoring Mtb replication and establishment of infection. Genes involved in cytosolic escape could be induced once bacterial numbers reach about 20 per cell which seems to be an important threshold to switch on the cell escape program of Mtb [30]. Gene deletions resulting in increased cytosolic translocation from vacuolar compartments have been reported for other bacteria; for example, the *sdhA* (a Dot/Icm-secreted effector) mutant of

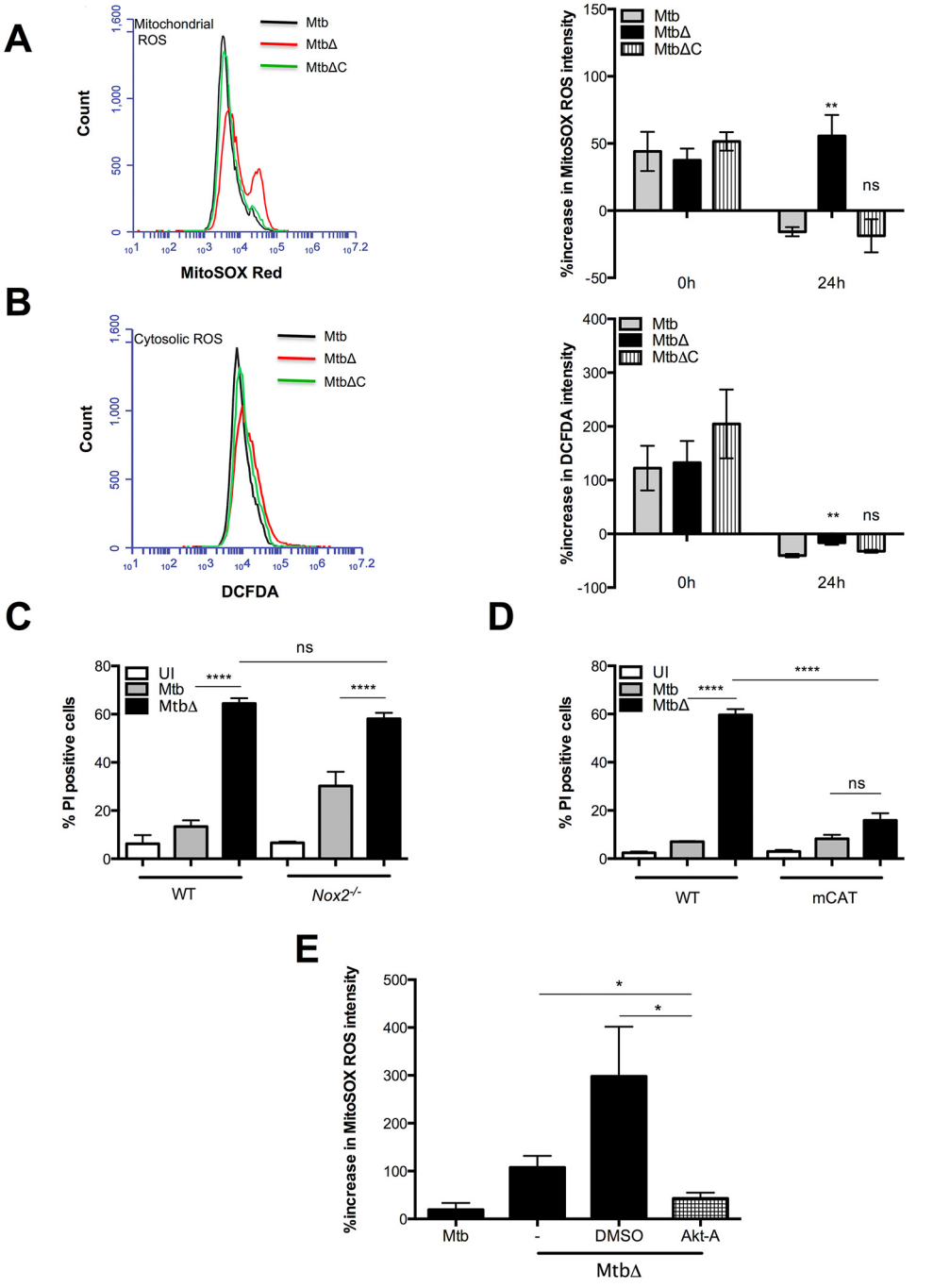

Fig 6. Mitochondrial ROS is required for cell death and autophagy induction by MtbΔ*Rv3167c*. Uninfected (UI), wild-type Mtb (Mtb), *Rv3167c* deletion mutant Mtb (MtbΔ) or complemented mutant Mtb (MtbΔC) bacteria infected cells were analyzed as described. (A) *Left*: Representative histogram of mitochondrial ROS measurement using MitoSOX Red staining of BMDMs at 24h. *Right*: Quantification of mitochondrial ROS by estimating increase in MitoSOX Red fluorescence intensity (mean ± S.E.M, n = 4) (B) *Left*: Representative histogram of cellular ROS measurement using DCFDA staining of BMDMs at 24h. *Right*: Quantification of cellular ROS by estimating increase in DCFDA fluorescence intensity (means ± S.E.M, n = 4). For (A) and (B), percentage increase in mean fluorescent intensity of infected cells compared to UI cells was calculated after subtracting background fluorescence. (C) Necrosis induction in WT and *Nox2*$^{-/-}$ BMDMs was determined by PI staining and flow cytometry at 48h (mean ± S.E.M, n = 6). (D) Necrosis induction in BMDMs from WT and mitochondrial targeted catalase (mCAT) knock-in mice was determined by PI staining and flow cytometry at 24h (mean ± S.E.M, n = 3). (E) Effect of the Akt activator sc-79 on mitochondrial ROS was measured by staining with MitoSOX Red and flowcytometry (mean ± S.E.M, n = 3).

doi:10.1371/journal.ppat.1005652.g006

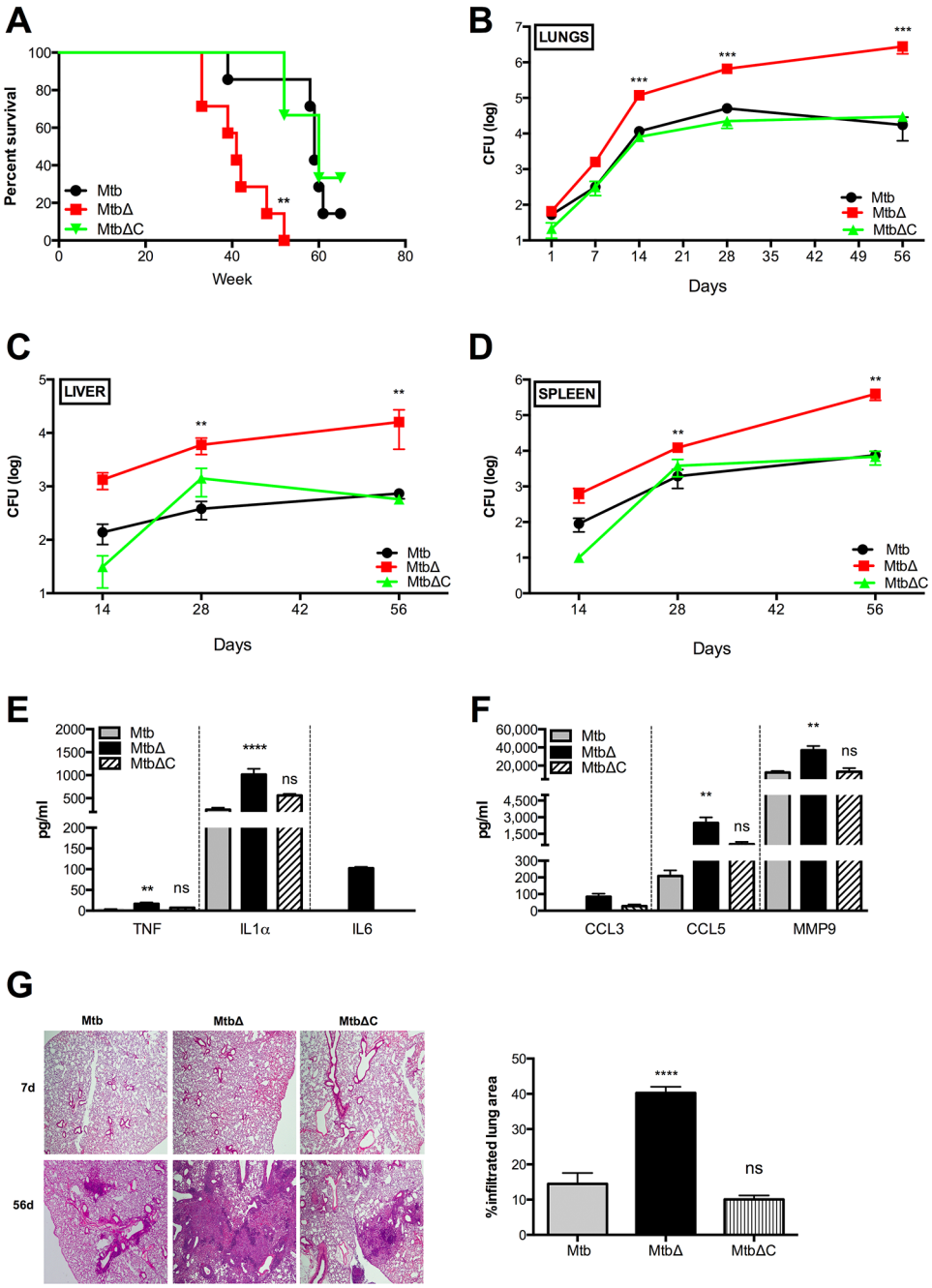

Fig 7. *Rv3167c* regulates virulence of Mtb. (A) Survival of C57Bl6 mice infected via the aerosol route with 100 CFU of wild-type Mtb (Mtb), *Rv3167c* deletion mutant Mtb (MtbΔ) or complemented mutant Mtb (MtbΔC) bacteria (n = 7 per experimental group) (B) Lung, (C) spleen and (D) liver bacterial burdens were determined at indicated times (mean ± S.E.M, n = 6) (E) Cytokines and (F) chemokines in lung tissue homogenates at 56d were quantified using a multiplex ELISA (mean ± S.E.M, n = 3). (G) *Left*: Representative image of H and E stained section of lung tissue. *Right*: Quantitative analysis of lung area exhibiting cellular infiltration at 56d performed using ImageJ (mean ± S.E.M, n = 3).

doi:10.1371/journal.ppat.1005652.g007

Legionella pneumophila and the *sifA* (an SPI2-secreted effector) mutant of *Salmonella typhimurium* [81,82]. Deletion of the secreted phospholipase A abrogated the early escape of the *L. pneumophila sdhA* mutant [81]. The Mtb genome encodes four phospholipases (*plc A-D*), which could potentially contribute to the early escape of Mtb*Δ*Rv3167c*. The mechanisms involved in Mtb escape from the phagosome and eventual induction of host cell necrosis to exit the cell are difficult to study because of the slow kinetic of the process. Consequently, the early induction of cytosolic escape and necrosis by Mtb*Δ*Rv3167c* make it a useful model to study the host cell escape mechanisms of Mtb.

The escape of Mtb from the phagosome to the cytosol is closely followed by necrotic death of the host cells [32,33,83]. Consistently, we measured higher levels of cell death by necrosis in Mtb*Δ*Rv3167c*-infected cells (Figs 1A, 1B and S9E). Mtb may induce necrosis via the manipulation of host cell lipid mediators by favoring the production of the eicosanoid LXA_4 [27]. In addition, the activation of the NLRP3-inflammasome was also shown to induce necrosis after Mtb infection [56]. We found that NLRP3 is dispensable for Mtb*Δ*Rv3167c*-mediated necrosis (S4C Fig). The regulation of cell death is complex and recently there have been major discoveries of signal transduction pathways for the regulation of programmed necrosis [1]. Using a combination of inhibitors and macrophages from knock-out mice, we screened for host factors required for Mtb*Δ*Rv3167c*-induced necrosis and ruled out the involvement of known programmed necrosis pathways (Figs 2, S4 and S5). Redundancy between the various necrosis-signaling modules may explain this result. For instance, both RIPK1-RIPK3 and caspase-1 activation are required for *S.tymphimurium*-induced necrotic cell death and blocking either one of the signaling pathways led only to a marginal inhibition of the death phenotype [43]. However, we found elevated mitochondrial ROS (mROS) to be required for the pro-necrotic phenotype of Mtb*Δ*Rv3167c* (Fig 6). Elevated mROS production could lead to increases in cytosolic ROS levels that may via lipid oxidation cause lysosomal permeabilization and cell death [1,84]. Lysosomal permeabilization has been implicated previously in necrosis induction by high bacillary loads of Mtb [61]. It is possible that Mtb*Δ*Rv3167c* may exploit a similar mechanism to kill host cells as increased lysosomal permeabilization was observed in cells infected with the mutant bacteria (Fig 2D). The Mm-mediated induction of necrosis after zebrafish infection also requires an increase in mROS [49]. Nevertheless, in contrast to our data (Figs 2A, S3B and S4A), Mm signals through the TNF/RIPK3 pathway to induce an increase of mROS and necrosis. The differences may reflect the variations in molecular pathogenesis pathways engaged by the human pathogen Mtb and the fish pathogen Mm.

Our data indicates involvement of diminished Akt activation in mitochondrial ROS generation in Mtb*Δ*Rv3167c*–infected cells (Fig 6E). The augmented phagosomal escape observed in Mtb*Δ*Rv3167c*-infected cells may allow for previously sequestered Mtb proteins to target mitochondria and trigger an increase in mROS generation. The mycobacterial type VII secretion system, ESX-5, is involved in the secretion of proteins containing Pro-Pro-Glu (PPE), Pro-Glu (PE) and polymorphic GC-rich sequences (PGRS) and has been implicated in cell lysis after Mtb escapes from the phagosome [39,85]. Interestingly, the ESX-5 substrates PE25 and PPE41 form a complex and induce necrosis [39,40]. Furthermore, the Mtb PE_PGRS33 protein, when ectopically expressed in a eukaryotic cell, localizes to the mitochondria and induces apoptotic and necrotic cell death [86]. The importance of these proteins in the context of infection with live bacteria has not been demonstrated yet. Another compelling target could be the secreted Mtb toxin CpnT which induces RIPK1-independent necrosis in Mtb-infected macrophages [87] via its NAD+ glycohydrolase activity [88].

It is possible that both mitochondrial localization of mycobacterial proteins and inhibition of Akt activation via Mtb proteins may both contribute to elevated mitochondrial ROS levels seen observed in Mtb*Δ*Rv3167c*-infected cells.

Autophagic clearance is a defense mechanism employed by host cells following detection of cytosolic pathogens. While macroautophagy (hereafter referred to as autophagy) is defined as the engulfment of cytosol by the autophagosome, selective autophagy describes the process in which autophagosome formation is directed towards a specific organelle, protein complex or microorganism by cargo receptor proteins (p62, NDP52, NBR1, Optineurin) [89–91]. Selective autophagy augments killing of intracellular mycobacteria, since reduced bacterial viability was seen following autophagy induction with IFNγ treatment of BCG-infected macrophages [92]. The relevance of selective autophagy for host defense against Mtb was demonstrated by the dramatically increased susceptibility of $Atg5^{-/-}$ mice when compared to wild-type mice [66,93]. It was thus unexpected that Mtb*Δ*Rv3167c* was hypervirulent in the mouse model (Fig 7A) even though increased autophagy induction was observed in Mtb*Δ*Rv3167c*-infected cells compared to Mtb-infected controls (Fig 3C and 3D). We found that while Mtb*Δ*Rv3167c* induces autophagy, there was no increase in selective autophagy, as very few mycobacteria (both wild-type and mutant) co-localized with autophagosomes (Fig 3A and 3B). Previous studies have shown that Mtb has evolved mechanisms to avoid recruitment into the autophagosome [66,72,94–96]. Our results support this observation and show that this immune evasion strategy remains intact in Mtb*Δ*Rv3167c*. The increased autophagy seen in Mtb*Δ*Rv3167c*-infected cells is most likely a host stress response to an increased number of cytosolic bacteria [66]. Autophagy may dampen inflammation by negative regulation of the inflammasome and via the degradation of danger associated molecular patterns during host cell necrosis [97,98]. $Atg5^{-/-}$ mice have higher basal level of inflammation when compared to wild-type mice [93] and Mtb-infected $Atg5^{-/-}$ mice had increased levels of pulmonary pro-inflammatory cytokines and exhibited increased lung tissue damage [66,99]. It is thus possible that in the absence of autophagy induction, the increased inflammatory response seen in Mtb*Δ*Rv3167c*-infected mice (Fig 7E and 7F) would have been even stronger.

Unlike apoptosis, which benefits the host by reducing mycobacterial viability, Mtb-induced necrosis is beneficial to the pathogen allowing it to exit from infected cells and to disseminate [14,100]. Consistent with this concept was our finding that the necrosis-inducing Mtb*Δ*Rv3167c* strain was hypervirulent in mice and guinea pig. The hypervirulence of various clinical Mtb strains and Mtb deletion mutants has been reported previously [101]. For example, the Beijing strain HN878 was found to be more virulent than another member of the same family in immunocompetent mice [102]. Deletion of the *mce1* operon, two component response regulators *KdpDE*, *tcrXY* and the serine threonine protein kinases *pknH*, *pknE* and *pknI* rendered Mtb hypervirulent in mouse studies [103–107]. The presence of multiple anti-virulence genes in Mtb gives rise to the question: why would Mtb encode genes that suppress its virulence? While virulence may be defined as the ability of a pathogen to cause disease, an important aspect of virulence is successful transmission between hosts [108]. As Mtb has probably co-evolved with humans for more than 50,000 years, moderation of its virulence would have prevented elimination of the early existent small host populations thus maximizing transmission opportunities and improving persistence of the pathogen [109,110].

Materials and Methods

Materials

THP1 monocytes were obtained from ATCC (TIB 202). GFP tagged LC3 expressing THP1 monocytes (THP1 LC3GFP) were provided by Dr. John Kehrl (NIH). THP1shASC and THP1shcontrol cells were obtained from Dr. Jenny Ting (University of North Carolina). C57Bl6, $Nox2^{-/-}$, $Casp3^{-/-}$ and mCAT transgenic mice were obtained from Jackson Laboratories. $Ripk3^{-/-}$ mice were obtained from Genentech. $Casp1/11^{-/-}$ mice were provided by Dr. Denise

Monack (Stanford School of Medicine). *Parp1*$^{-/-}$ mice were obtained from Dr. Ted Dawson (Johns Hopkins University). *Tnfr1*$^{-/-}$, *Il1r1*$^{-/-}$, *Irf3*$^{-/-}$ and *Ifnβ*$^{-/-}$ mice were provided by Dr. Alan Sher (NIH). Immortalized wildtype, *Nlrp3*$^{-/}$ and *Trif*$^{-/-}$*MyD88*$^{-/-}$ BMDMs were provided by Dr. Igor Brodsky (University of Pennsylvania). Atg5$^{fl/fl}$ LysM Cre^{+} (Atg5$^{-/-}$) and Atg5$^{fl/fl}$ LysM Cre^{-} (Atg5$^{+/+}$) mice were obtained from Dr. Herbert Virgin IV (Washington University School of Medicine). zVAD FMK, Necrostatin 1, MAPK inhibitors (SP600125, SB203580), Akt activator (sc-79) and DPI were purchased from Calbiochem. BafilomycinA1, glutathione and N-acetyl cysteine were sourced from Sigma. 3-MA was purchased from Tocris Biosciences.

Generation of mutant and complement strains

Rv3167c was deleted in *M. tuberculosis* H37Rv using a specialized phage transduction strategy described previously [111]. Gene deletion was confirmed by RT-PCR as well as by southern blotting. The probes used were labeled with biotin using BrightStar Psoralen-Biotin Kit. Genomic DNA was digested with EcoRI. The DNA fragments were separated by agarose gel electrophoresis, transferred to charged nylon membrane, and denatured with 0.4N NaOH. The probe was denatured at 90°C for 10 min in the presence of 10mM EDTA and hybridized to the membrane at 55°C for 16h in hybridization buffer (AlkPhos Direct hybridization buffer with 0.5M NaCl). The membrane was washed and the probe was detected using a BrightStar BioDetect Nonisotopic Detection Kit. For generating the complement strain, *Rv3167c* gene sequence including 60bp upstream was cloned into the episomal plasmid pMV261, electroporated into the *Rv3167c* mutant strain and plated on 7H10 plates with 40μg/ml kanamycin.

Bacterial culture

Bacterial strains were grown in 7H9 medium supplemented with 10% ADC, 0.5% glycerol and 0.05% Tween 80. Hygromycin (50μg/ml) and kanamycin (40μg/ml) were added to the mutant and complement cultures respectively. For infection, cultures with an OD_{600} between 0.6–0.8 (corresponding to the late log phase of growth) were pelleted and resuspended in 0.05% PBS-Tween 80 prior to addition to cells.

Determination of *in vitro* and *ex vivo* bacterial growth rate

To measure *in vitro* bacterial growth, bacteria were added to 7H9 medium to obtain a starting OD_{600} of 0.01. OD_{600} measurements were made at 24h intervals until 7 days. *Ex vivo* bacterial growth was determined by infecting THP1 macrophages and lysing them at the indicated timepoints with 0.1% Triton X 100. Appropriate dilutions were plated on 7H11 medium in triplicate. Inoculated plates were incubated at 37°C and colonies were counted approximately 2 weeks after plating.

Cell culture and infection

THP1 monocytes were maintained in RPMI 1640 supplemented with 10% heat inactivated FCS. Cells were differentiated with 20ng/ml PMA for 20–24 hours, washed and infected in growth medium containing 5% human serum. Bacteria were added to cells at MOI 3 for 4 hours at 37°C, extracellular bacteria were removed by PBS washes and chase medium containing 100μg/ml gentamicin was added. BMDMs were prepared from cells obtained from femurs and tibia of various mouse strains and cultured in DMEM supplemented with 10% heat inactivated FCS, 25% L929 supernatant and 1% Penicillin-Streptomycin. Growth medium was replaced with DMEM containing 10% non-heat inactivated FCS for 4h and cells were infected at MOI 10 in same medium in the manner described above. Chase media contained 10% L929

supernatant in order to avoid cell death induction due to cytokine withdrawal. Immortalized BMDMs were maintained in DMEM containing 10% heat inactivated FCS and infected in media similar to that used for primary BMDMs. Human monocyte derived macrophages (hMDMs) were prepared from elutriated monocyte fractions obtained from NIH blood bank. Monocyte fractions were seeded in serum free RPMI for one hour. Non-adherent cells were removed and adherent cells were differentiated in RPMI medium containing 5% off-the-clot AB human serum (Gemini) and 10ng/ml human MCSF (Peprotech) for 7 days. Inhibitors (with the exception of 3-MA) were added to cells one hour prior to infection and included in chase medium. 3-MA was added only to chase medium. For all experiments, 0h time point refers to end of infection period when cells have been exposed to bacteria for 4 hours.

Cell death assays

Cells were stained with 1μg/ml propidium iodide (PI) (Sigma-Aldrich) for 10 minutes at room temperature and analyzed by flowcytometry. For TUNEL stain, cells were fixed in 4% paraformaldehyde overnight, stained as per manufacturer's instructions (Roche) and examined by either flow cytometry or fluorescence microscopy. Hypodiploid stain was performed using PI/RNase staining buffer (BD Pharmingen) following overnight fixation in 70% ethanol as per manufacturer's instructions. For all flow cytometry analyses, at least 10,000 cells were acquired (BD Accuri C6). Toxilight assay to measure adenylate kinase release from cells was performed as per manufacturers instructions.

Autophagy analysis

Autophagy induction in THP1 LC3GFP expressing cells was analyzed as described previously [67]. Briefly, cells were permeabilized with 0.05% saponin for 5 minutes, washed and resuspended in PBS containing 5% FCS. Permeabilization resulted in loss of cytosolic LC3I while LC3II bound to autophagosome membranes were retained, which was measured by flow cytometry (50,000 cells acquired, BD Accuri C6). For immunofluorescence analysis, bacteria were stained with 0.4mg/ml AF647-NHS ester (Molecular Probes) in 0.1M sodium bicarbonate solution for 30 minutes at 37°C and used for infecting cells on slides. At specified time points, cells were fixed with 4% paraformaldehyde overnight, stained with Hoechst 33342 and analyzed by confocal microscopy (Zeiss LSM710).

Immunoblotting

Cell lysates were obtained by lysing cells with RIPA buffer containing protease (Complete, Mini EDTA free, Roche) and phosphatase inhibitor cocktails (PhosStop, Roche) followed by centrifugation at 12,000g for 5 minutes. Pierce BCA protein assay kit (Thermo Scientific) was used to measure protein concentrations to ensure equivalent loading. Antibodies against phosphorylated and total Akt and MAPKs, PARP, tubulin and GFP were purchased from Cell Signaling and used at 1:1000 dilution. Anti LC3 antibody was purchased from Epitomics and used at 1:2500 dilution. Densitometric analysis was performed using ImageJ software.

CCF4 FRET assay

To detect mycobacterial escape from the phagosome, the CCF4 FRET assay was performed as described previously [34]. Briefly, cells were stained with 8μM of CCF4 (Invitrogen) in EM buffer (120mM NaCl, 7mM KCl, 1.8mM $CaCl_2$, 0.8mM $MgCl_2$ 5mM glucose, 25mM Hepes, pH7.3) containing 2.5μM of probenecid (Sigma-Aldrich) for 1.5 hours at room temperature. Live populations were distinguished from dead ones by addition of Live/Dead Fixable Red

stain (Invitrogen) for 30 minutes at room temperature. After staining cells were fixed with 4% PFA overnight and analyzed by flow cytometry (BD FACS CantoII). 40,000 cells were acquired and post acquisition analysis done using FlowJo software (Treestar, OR). For estimation of bacterial β-lactamase activity, bacteria were resuspended in PBS containing 50μg/ml porcine esterase liver extract and 100nM CCF4-AM and incubated at 37°C for 12h. Fluoresence measurements were made using Biotek Synergy 4 microplate reader.

Measurement of ROS generation

For measurement of ROS levels in BMDMs, cells were infected as described previously [78]. At indicated time points after infection, cells were harvested and stained with 10μM CM-H2DCFDA (Molecular Probes) or 1.25μM MitoSOX Red (Molecular Probes) for 30 minutes at 37°C in HBSS. Cells were analyzed by flow cytometry (at least 10,000 cells acquired, BD Accuri C6) after HBSS wash.

$DIOC_6$ staining

Cells were stained with 40 nmol of $DIOC_6$ stain (Molecular Probes) at 37°C for 15 minutes, washed and analyzed by flow cytometry (10,000 cells acquired, BD Accuri C6).

Electron microscopy

THP1 cells were fixed in 2% gluteraldehyde and 2% paraformaldehyde in 0.1M sodium cacodylate buffer pH7.4 for 1 hour. They were carefully pelleted and re-suspended in 2% paraformaldehyde for several hours, followed by rinsing in 0.1M sodium cacodylate buffer and pelleted in 2% agar in the same buffer. The samples were post fixed in 1% osmium tetroxide in 0.1M sodium cacodylate buffer, rinsed in distilled water and, en bloc stained in 2% aqueous uranyl acetate for a further hour. They were then rinsed and dehydrated in an ethanol series (50% to 100%) followed by resin infiltration Embed 812 (Electron Microscopy Sciences) and baked overnight at 60°C. Hardened blocks were cut using a Leica UltraCut UC7. 60nm sections were collected on formvar/carbon coated nickel grids and contrast stained using 2% uranyl acetate and lead citrate. Grids were all viewed in a FEI Tencai Biotwin TEM at 80Kv. Images were taken using Morada CCD and iTEM (Olympus) software.

Embedding and sectioning was performed at the electron microscopy core facility at the Yale School of Medicine.

Animal studies

C57Bl/6 mice were infected with 100 CFU of each of the various bacterial strains grown to late log phase via the aerosol route using a Glas-Col full body inhalation exposure system. At the indicated time points, 3 mice per group were sacrificed and bacterial load was determined by homogenizing the organs in PBS and plating serial dilutions on 7H11 plates. Lung homogenate supernatants were used for cytokine analysis using the Luminex MAGPIX platform (R&D Bioscience). Superior lobes of the lungs were fixed in 10% buffered formalin for histopathology. Paraffin embedding, sectioning and hematoxylin and eosin (H and E) staining were performed by AML Labs, Baltimore. Total lung area and areas of inflamed regions in H and E stained lung sections were quantified using ImageJ.

Female outbred Hartley guinea pigs (250-300g) were purchased from Charles River Labs (Wilmington, MA). Animals were infected with each of the three Mtb strains via aerosol using a Madison chamber aerosol generation device (University of Wisconsin, Madison, WI) calibrated to deliver ~3 $\log_{10}$ CFU in the lungs. Four animals from each group were sacrificed on

day 1 and day 28 post-infection. The lungs were homogenized, as previously described, and the lung homogenates were plated on 7H11 Middlebrook agar and incubated at 37°C for 4 weeks before final CFU counts were determined [112].

Alveolar macrophages were harvested by bronchoalveolar lavage (BAL) as described previously [113]. Briefly, cold PBS with 3% FCS was instilled into the lungs following insertion into the trachea of an 18-gauge cannula fixed to a 20-ml syringe. The cells were pelleted by centrifugation at 380g for 10 min, washed twice with RPMI-1640 supplemented with 10% FCS, and 10μM 2-mercaptoethanol (RPMI complete medium), and resuspended in 1 ml RPMI complete medium. Following transport from Johns Hopkins to University of Maryland on ice, viable cells were enumerated by the trypan blue exclusion method and seeded in RPMI complete medium overnight. Adherent cells were infected in RPMI medium containing 5% FCS at specified MOI for 4 hours at 37°C, extracellular bacteria were removed by PBS washes and chase medium containing 100μg/ml gentamicin was added.

Statistical analysis

Statistical analysis was performed using GraphPad Prism version 6.0 software. Data is presented as mean ± S.E.M. of three independent experiments and one-way ANOVA with Tukey post-test was used unless mentioned otherwise in the figure legends. p-value significance is as follows—*- ≤0.05, ** - ≤0.01, *** - ≤0.001, **** - 0.0001.

Ethics statement

All animals were handled in accordance with the NIH guidelines for housing and care of laboratory animals and the studies were approved by the Institutional Animal Care and Use Committees at the University of Maryland, College Park (protocol no—R-12-55) and Johns Hopkins University School of Medicine (protocol no—GP12M88).

Supporting Information

S1 Fig. Identification of *Rv3167c* as an anti cell death gene. (A) Insert of cosmid J21. Position of deletion mutants that induce higher cell death compared to Mtb indicated. The 7/10 region contains *Rv3167c*. The image has been adapted from the Tuberculist website (B) Cell death induction by Mtb deletion mutants in the J21 cosmid determined by TUNEL staining and flow cytometry (mean ± S.E.M, n = 6) (C) Screening of individual gene deletion mutants in the 7/10 region of the J21 cosmid for increased cell death induction compared to Mtb performed by TUNEL staining and flow cytometry (mean ± S.E.M, n = 3).
(TIF)

S2 Fig. Generation of *Rv3167c* mutant (MtbΔ*Rv3167c*) in Mtb. (A) A hygromycin cassette was introduced into the Mtb H37Rv genome by specialized transduction to generate MtbΔ*Rv3167c*. An episomal plasmid with *Rv3167c* expression under the control of a constitutively active promoter was used to generate the complement strain MtbΔ*Rv3167c*-C. The sizes of fragments obtained after digestion of genomic DNA with EcoRI and using a specific probe for southern blotting are indicated. (B) Knockout and complementation of *Rv3167c* was confirmed by southern blotting. (C) Deletion of *Rv3167c* confirmed by RT-PCR. A non-related mutant (Δ3165c) was used as a control to demonstrate primer specificity. (D) Replication of bacterial strains *ex vivo* was determined by lysing infected THP1 cells and plating lysates on 7H11 medium at indicated times (mean ± S.E.M, n = 9). (E) *In vitro* growth rate of bacterial strains in 7H9 medium was measured every 24h (mean ± S.E.M, n = 9).
(TIFF)

S3 Fig. Efficacy of zVAD fmk and Necrostatin-1. (A) Efficacy of the pan caspase inhibitor zVAD-fmk (40μM) was assessed by inhibition of camptothecin-mediated apoptosis in THP1 cells measured by TUNEL staining and flow cytometry (mean ± S.E.M, n = 3). (B) BMDMs were treated with the RIPK1 inhibitor necrostatin-1 (Nec1) (100μM) one hour prior to and throughout the infection and necrosis induction measured by PI staining at 24h (mean ± S.E.M, n = 3). (C) Necrostatin-1 (Nec1, 100μM) efficacy was determined by inhibition of LPS and zVAD-fmk induced cell death (RIPK1 dependent) in BMDMs measured by PI staining and flowcytometry (mean ± S.E.M, n = 3). (D) *RipK3*$^{-/-}$ BMDMs were treated with the pan caspase inhibitor zVAD FMK one hour prior to and throughout the infection and necrosis induction measured by PI staining at 24h (mean ± S.E.M, n = 3).
(TIFF)

S4 Fig. Mtb*Δ*Rv3167c mediated necrosis is independent of TNF, IL1, NLRP3 inflammasome and type I IFN. (A) Necrosis induction in WT and *Tnfr1*$^{-/-}$ BMDMs was determined by PI staining and flow cytometry at 72h (mean ± S.E.M, n = 3). (B) Necrosis induction in WT and *IL1r1*$^{-/-}$ BMDMs was determined by PI staining and flow cytometry at 72h (mean ± S.E.M, n = 6). (C) Necrosis induction in immortalized WT and *Nlrp3*$^{-/-}$ BMDMs was determined by PI staining and flow cytometry at 24h (mean ± S.E.M, n = 3). (D) Necrosis induction in THP1 shASC and control cells was determined by Toxilight assay at 48h (mean ± S.E.M, n = 9) (E) Necrosis induction in WT and *Irf3*$^{-/-}$ BMDMs was determined by PI staining and flow cytometry at 48h (mean ± S.E.M, n = 3) (F) Necrosis induction in WT and *Ifnβ*$^{-/-}$ BMDMs was determined by PI staining and flow cytometry at 48h (mean ± S.E.M, n = 8).
(TIFF)

S5 Fig. Mtb*ΔRv3167c* mediated necrosis is independent of TLR signaling. Necrosis induction in (A) WT and *Trif*$^{-/-}$, (B) WT and *MyD88*$^{-/-}$ and (C) immortalized WT and *Trif*$^{-/-}$ *MyD88*$^{-/-}$ BMDM's was determined by PI staining and flow cytometry at 48h (mean ± S.E.M, n = 3).
(TIFF)

S6 Fig. Mtb*Δ*Rv3167c does not inhibit autophagosome maturation. (A) Accumulation of LC3II GFP in Mtb*Δ*Rv3167c* infected THP1 LC3GFP cells treated with Bafilomycin (BafA1, 250nM) examined by flow cytometry at 16h (mean ± S.E.M, n = 6). (B) Free GFP generated during lysosomal degradation of LC3II GFP detected by western blotting in whole cell lysates. Image is representative of three independent experiments. (C) Necrosis induction in presence of autophagy inhibitor 3-MA was determined by Toxilight assay at 24h (mean ± S.E.M, n = 4).
(TIF)

S7 Fig. Mtb, Mtb*Δ*Rv3167c and Mtb*Δ*Rv3167c*-C have similar β-lactamase activity *in vitro*. β-lactamase activity of the indicated bacterial strains was determined by incubating bacterial cultures with CCF4-AM and measuring fluorescence emission at 450nm and 535nm. Data is represented as fold change over CCF4-AM incubated in absence of bacteria. ΔblaC is a *blaC* deleted H37Rv strain [114].
(TIFF)

S8 Fig. Necrosis and autophagy induction by Mtb*Δ*Rv3167c is dependent on ROS. (A) Effect of the flavoprotein inhibitor DPI (10μM) on necrosis induction in THP1 cells was determined by the Toxilight assay at 24h (mean ± S.E.M, n = 6). (B) Effect of the antioxidants glutathione (15mM) and N-acetyl cysteine (NAC, 10mM) on necrosis induction in THP1 cells was determined by TUNEL staining and fluorescence microscopy at 24h (mean ± S.E.M, n = 9). (C) Loss of mitochondrial membrane potential was determined by $DIOC_6$ staining at the indicated

time points (mean ± S.E.M, n = 9). (D) Effect of DPI (10μM) on autophagy induction in THP1 LC3GFP cells was determined by flow cytometry (mean ± S.E.M, n = 6).
(TIFF)

S9 Fig. Mtb*Δ*Rv3167c is hypervirulent in SCID mice and guinea pigs. (A) Survival of SCID mice infected via the aerosol route with 100 CFU of bacteria (n = 5). (B) Bacterial uptake by SCID mice was determined by plating lung homogenates prepared at day 1 (mean ± S.E.M, n = 3). (C) Guinea pigs were infected via aerosol route. Bacterial uptake by guinea pigs was determined by plating lung homogenates prepared at 1d (means ± S.E.M, n = 4). (D) Lung burden in guinea pigs at 28 days (mean ± S.E.M, n = 4). (E) Cell death induction by Mtb*Δ*Rv3167c in guinea pig alveolar macrophages infected *ex vivo* was determined by TUNEL staining and microscopy (mean ± S.E.M, n = 3).
(TIF)

Acknowledgments

We thank Tim Maugel (UMD) and the CCMI EM Core Facility, Yale School of Medicine for their help with electron microscopy imaging and quantification. We thank Jeff Quigley and Sarah Ahlbrand for critical discussions and help with manuscript preparation.

Author Contributions

Conceived and designed the experiments: LS SAG VB. Performed the experiments: LS SAG BEH JLM. Analyzed the data: LS VB. Contributed reagents/materials/analysis tools: PCK. Wrote the paper: LS VB.

References

1. Vanden Berghe T, Linkermann A, Jouan-Lanhouet S, Walczak H, Vandenabeele P. Regulated necrosis: the expanding network of non-apoptotic cell death pathways. Nat Rev Mol Cell Biol. 2014; 15: 135–147. doi: 10.1038/nrm3737 PMID: 24452471
2. Galluzzi L, Vitale I, Abrams JM, Alnemri ES, Baehrecke EH, Blagosklonny MV, et al. Molecular definitions of cell death subroutines: recommendations of the Nomenclature Committee on Cell Death 2012. Cell Death Differ. Nature Publishing Group; 2011; 19: 107–120. doi: 10.1038/cdd.2011.96
3. Lamkanfi M, Dixit VM. Manipulation of host cell death pathways during microbial infections. Cell Host and Microbe. 2010; 8: 44–54. doi: 10.1016/j.chom.2010.06.007 PMID: 20638641
4. Upton JW, Chan FK-M. Staying alive: cell death in antiviral immunity. Mol Cell. 2014; 54: 273–280. doi: 10.1016/j.molcel.2014.01.027 PMID: 24766891
5. Sridharan H, Upton JW. Programmed necrosis in microbial pathogenesis. Trends in microbiology. 2014; 22: 199–207. doi: 10.1016/j.tim.2014.01.005 PMID: 24565922
6. Upton JW, Kaiser WJ, Mocarski ES. Virus inhibition of RIP3-dependent necrosis. Cell Host and Microbe. 2010; 7: 302–313. doi: 10.1016/j.chom.2010.03.006 PMID: 20413098
7. Rodrigue-Gervais IG, Labbé K, Dagenais M, Dupaul-Chicoine J, Champagne C, Morizot A, et al. Cellular inhibitor of apoptosis protein cIAP2 protects against pulmonary tissue necrosis during influenza virus infection to promote host survival. Cell Host and Microbe. 2014; 15: 23–35. doi: 10.1016/j.chom.2013.12.003 PMID: 24439895
8. Li S, Zhang L, Yao Q, Li L, Dong N, Rong J, et al. Pathogen blocks host death receptor signalling by arginine GlcNAcylation of death domains. Nature. 2013; 501: 242–246. doi: 10.1038/nature12436 PMID: 23955153
9. Pearson JS, Giogha C, Ong SY, Kennedy CL, Kelly M, Robinson KS, et al. A type III effector antagonizes death receptor signalling during bacterial gut infection. Nature. Nature Publishing Group; 2013; 501: 247–251. doi: 10.1038/nature12524
10. Di Paolo NC, Doronin K, Baldwin LK, Papayannopoulou T, Shayakhmetov DM. The Transcription Factor IRF3 Triggers "Defensive Suicide" Necrosis in Response to Viral and Bacterial Pathogens. Cell Reports. 2013; 3: 1840–1846. doi: 10.1016/j.celrep.2013.05.025 PMID: 23770239

11. Briken V, Miller JL. Living on the edge: inhibition of host cell apoptosis by Mycobacterium tuberculosis. Future Microbiology. 2008; 3: 415–422. doi: 10.2217/17460913.3.4.415 PMID: 18651813

12. Moraco AH, Kornfeld H. Cell death and autophagy in tuberculosis. Semin Immunol. 2014; 26: 497–511. doi: 10.1016/j.smim.2014.10.001 PMID: 25453227

13. Ramakrishnan L. Revisiting the role of the granuloma in tuberculosis. Nat Rev Immunol. 2012; 12: 352–366. doi: 10.1038/nri3211 PMID: 22517424

14. Behar SM, Divangahi M, Remold HG. Evasion of innate immunity by Mycobacterium tuberculosis: is death an exit strategy? Nat Rev Micro. 2010; 8: 668–674. doi: 10.1038/nrmicro2387

15. Velmurugan K, Chen B, Miller JL, Azogue S, Gurses S, Hsu T, et al. Mycobacterium tuberculosis nuoG is a virulence gene that inhibits apoptosis of infected host cells. PLoS Pathog. 2007; 3: e110. doi: 10.1371/journal.ppat.0030110 PMID: 17658950

16. Jayakumar D, Jacobs WR, Narayanan S. Protein kinase E of Mycobacterium tuberculosis has a role in the nitric oxide stress response and apoptosis in a human macrophage model of infection. Cell Microbiol. 2008; 10: 365–374. doi: 10.1111/j.1462-5822.2007.01049.x PMID: 17892498

17. Hinchey J, Lee S, Jeon BY, Basaraba RJ, Venkataswamy MM, Chen B, et al. Enhanced priming of adaptive immunity by a proapoptotic mutant of Mycobacterium tuberculosis. J Clin Invest. 2007; 117: 2279–2288. doi: 10.1172/JCI31947 PMID: 17671656

18. Danelishvili L, Yamazaki Y, Selker J, Bermudez LE. Secreted Mycobacterium tuberculosis Rv3654c and Rv3655c proteins participate in the suppression of macrophage apoptosis. PLoS ONE. 2010; 5: e10474. doi: 10.1371/journal.pone.0010474 PMID: 20454556

19. Sun J, Singh V, Lau A, Stokes RW, Obregón-Henao A, Orme IM, et al. Mycobacterium tuberculosis nucleoside diphosphate kinase inactivates small GTPases leading to evasion of innate immunity. Salgame P, editor. PLoS Pathog. 2013; 9: e1003499. doi: 10.1371/journal.ppat.1003499 PMID: 23874203

20. Pan H, Yan B-S, Rojas M, Shebzukhov YV, Zhou H, Kobzik L, et al. Ipr1 gene mediates innate immunity to tuberculosis. Nature. 2005; 434: 767–772. doi: 10.1038/nature03419 PMID: 15815631

21. Martin CJ, Booty MG, Rosebrock TR, Nunes-Alves C, Desjardins DM, Keren I, et al. Efferocytosis is an innate antibacterial mechanism. Cell Host and Microbe. 2012; 12: 289–300. doi: 10.1016/j.chom.2012.06.010 PMID: 22980326

22. Yang C-T, Cambier CJ, Davis JM, Hall CJ, Crosier PS, Ramakrishnan L. Neutrophils exert protection in the early tuberculous granuloma by oxidative killing of mycobacteria phagocytosed from infected macrophages. Cell Host and Microbe. 2012; 12: 301–312. doi: 10.1016/j.chom.2012.07.009 PMID: 22980327

23. Schaible UE, Winau F, Sieling PA, Fischer K, Collins HL, Hagens K, et al. Apoptosis facilitates antigen presentation to T lymphocytes through MHC-I and CD1 in tuberculosis. Nat Med. 2003; 9: 1039–1046. doi: 10.1038/nm906 PMID: 12872166

24. Divangahi M, Desjardins D, Nunes-Alves C, Remold HG, Behar SM. Eicosanoid pathways regulate adaptive immunity to Mycobacterium tuberculosis. Nat Immunol. 2010; 11: 751–758. doi: 10.1038/ni.1904 PMID: 20622882

25. Divangahi M, Chen M, Gan H, Desjardins D, Hickman TT, Lee DM, et al. Mycobacterium tuberculosis evades macrophage defenses by inhibiting plasma membrane repair. Nat Immunol. 2009; 10: 899–906. doi: 10.1038/ni.1758 PMID: 19561612

26. Bafica A, Scanga CA, Serhan C, Machado F, White S, Sher A, et al. Host control of Mycobacterium tuberculosis is regulated by 5-lipoxygenase-dependent lipoxin production. J Clin Invest. 2005; 115: 1601–1606. doi: 10.1172/JCI23949 PMID: 15931391

27. Chen M, Divangahi M, Gan H, Shin DSJ, Hong S, Lee DM, et al. Lipid mediators in innate immunity against tuberculosis: opposing roles of PGE2 and LXA4 in the induction of macrophage death. J Exp Med. 2008; 205: 2791–2801. doi: 10.1084/jem.20080767 PMID: 18955568

28. Tobin DM, Roca FJ, Oh SF, McFarland R, Vickery TW, Ray JP, et al. Host genotype-specific therapies can optimize the inflammatory response to mycobacterial infections. Cell. 2012; 148: 434–446. doi: 10.1016/j.cell.2011.12.023 PMID: 22304914

29. Tobin DM, Vary JC, Ray JP, Walsh GS, Dunstan SJ, Bang ND, et al. The lta4h locus modulates susceptibility to mycobacterial infection in zebrafish and humans. Cell. 2010; 140: 717–730. doi: 10.1016/j.cell.2010.02.013 PMID: 20211140

30. Repasy T, Lee J, Marino S, Martinez N, Kirschner DE, Hendricks G, et al. Intracellular bacillary burden reflects a burst size for Mycobacterium tuberculosis in vivo. PLoS Pathog. 2013; 9: e1003190. doi: 10.1371/journal.ppat.1003190 PMID: 23436998

31. Welin A, Eklund D, Stendahl O, Lerm M. Human macrophages infected with a high burden of ESAT-6-expressing M. tuberculosis undergo caspase-1- and cathepsin B-independent necrosis. PLoS ONE. 2011; 6: e20302. doi: 10.1371/journal.pone.0020302 PMID: 21637850

32. van der Wel N, Hava D, Houben D, Fluitsma D, van Zon M, Pierson J, et al. M. tuberculosis and M. leprae translocate from the phagolysosome to the cytosol in myeloid cells. Cell. 2007; 129: 1287–1298. doi: 10.1016/j.cell.2007.05.059 PMID: 17604718

33. Simeone R, Bobard A, Lippmann J, Bitter W, Majlessi L, Brosch R, et al. Phagosomal rupture by Mycobacterium tuberculosis results in toxicity and host cell death. PLoS Pathog. 2012; 8: e1002507. doi: 10.1371/journal.ppat.1002507 PMID: 22319448

34. Simeone R, Sayes F, Song O, Gröschel MI, Brodin P, Brosch R, et al. Cytosolic Access of Mycobacterium tuberculosis: Critical Impact of Phagosomal Acidification Control and Demonstration of Occurrence In Vivo. Salgame P, editor. PLoS Pathog. 2015; 11: e1004650. doi: 10.1371/journal.ppat.1004650 PMID: 25658322

35. Gao L-Y, Guo S, McLaughlin B, Morisaki H, Engel JN, Brown EJ. A mycobacterial virulence gene cluster extending RD1 is required for cytolysis, bacterial spreading and ESAT-6 secretion. Mol Microbiol. 2004; 53: 1677–1693. doi: 10.1111/j.1365-2958.2004.04261.x PMID: 15341647

36. Volkman HE, Pozos TC, Zheng J, Davis JM, Rawls JF, Ramakrishnan L. Tuberculous granuloma induction via interaction of a bacterial secreted protein with host epithelium. Science. American Association for the Advancement of Science; 2010; 327: 466–469. doi: 10.1126/science.1179663

37. Aguilo JI, Alonso H, Uranga S, Marinova D, Arbués A, de Martino A, et al. ESX-1-induced apoptosis is involved in cell-to-cell spread of Mycobacterium tuberculosis. Cell Microbiol. 2013. doi: 10.1111/cmi.12169

38. Houben D, Demangel C, van Ingen J, Perez J, Baldeón L, Abdallah AM, et al. ESX-1-mediated translocation to the cytosol controls virulence of mycobacteria. Cell Microbiol. 2012; 14: 1287–1298. doi: 10.1111/j.1462-5822.2012.01799.x PMID: 22524898

39. Abdallah AM, Bestebroer J, Savage NDL, de Punder K, van Zon M, Wilson L, et al. Mycobacterial secretion systems ESX-1 and ESX-5 play distinct roles in host cell death and inflammasome activation. J Immunol. 2011; 187: 4744–4753. doi: 10.4049/jimmunol.1101457 PMID: 21957139

40. Tundup S, Mohareer K, Hasnain SE. Mycobacterium tuberculosis PE25/PPE41 protein complex induces necrosis in macrophages: Role in virulence and disease reactivation? FEBS Open Bio. Elsevier; 2014; 4: 822–828. doi: 10.1016/j.fob.2014.09.001

41. Vega-Manriquez X, López-Vidal Y, Moran J, Adams LG, Gutiérrez-Pabello JA. Apoptosis-inducing factor participation in bovine macrophage Mycobacterium bovis-induced caspase-independent cell death. Infection and Immunity. 2007; 75: 1223–1228. doi: 10.1128/IAI.01047-06 PMID: 17158896

42. Baritaud M, Cabon L, Delavallée L, Galán-Malo P, Gilles M-E, Brunelle-Navas M-N, et al. AIF-mediated caspase-independent necroptosis requires ATM and DNA-PK-induced histone H2AX Ser139 phosphorylation. Cell Death Dis. 2012; 3: e390. doi: 10.1038/cddis.2012.120 PMID: 22972376

43. Robinson N, McComb S, Mulligan R, Dudani R, Krishnan L, Sad S. Type I interferon induces necroptosis in macrophages during infection with Salmonella enterica serovar Typhimurium. Nat Immunol. 2012; 13: 954–962. doi: 10.1038/ni.2397 PMID: 22922364

44. Lee J, Remold HG, Ieong MH, Kornfeld H. Macrophage apoptosis in response to high intracellular burden of Mycobacterium tuberculosis is mediated by a novel caspase-independent pathway. J Immunol. 2006; 176: 4267–4274. PMID: 16547264

45. Vandenabeele P, Declercq W, Van Herreweghe F, Vanden Berghe T. The role of the kinases RIP1 and RIP3 in TNF-induced necrosis. Sci Signal. 2010; 3: re4–re4. doi: 10.1126/scisignal.3115re4 PMID: 20354226

46. Wang Z, Jiang H, Chen S, Du F, Wang X. The mitochondrial phosphatase PGAM5 functions at the convergence point of multiple necrotic death pathways. Cell. 2012; 148: 228–243. doi: 10.1016/j.cell.2011.11.030 PMID: 22265414

47. Chen X, Li W, Ren J, Huang D, He W-T, Song Y, et al. Translocation of mixed lineage kinase domain-like protein to plasma membrane leads to necrotic cell death. Cell Res. 2014; 24: 105–121. doi: 10.1038/cr.2013.171 PMID: 24366341

48. Wang H, Sun L, Su L, Rizo J, Liu L, Wang L-F, et al. Mixed lineage kinase domain-like protein MLKL causes necrotic membrane disruption upon phosphorylation by RIP3. Mol Cell. 2014; 54: 133–146. doi: 10.1016/j.molcel.2014.03.003 PMID: 24703947

49. Roca FJ, Ramakrishnan L. TNF dually mediates resistance and susceptibility to mycobacteria via mitochondrial reactive oxygen species. Cell. 2013; 153: 521–534. doi: 10.1016/j.cell.2013.03.022 PMID: 23582643

50. He S, Liang Y, Shao F, Wang X. Toll-like receptors activate programmed necrosis in macrophages through a receptor-interacting kinase-3-mediated pathway. Proceedings of the National Academy of Sciences. National Acad Sciences; 2011; 108: 20054–20059. doi: 10.1073/pnas.1116302108

51. Virág L, Robaszkiewicz A, Rodriguez-Vargas JM, Oliver FJ. Poly(ADP-ribose) signaling in cell death. Mol Aspects Med. 2013; 34: 1153–1167. doi: 10.1016/j.mam.2013.01.007 PMID: 23416893

52. Moubarak RS, Yuste VJ, Artus C, Bouharrour A, Greer PA, Menissier-de Murcia J, et al. Sequential activation of poly(ADP-ribose) polymerase 1, calpains, and Bax is essential in apoptosis-inducing factor-mediated programmed necrosis. Molecular and Cellular Biology. American Society for Microbiology; 2007; 27: 4844–4862. doi: 10.1128/MCB.02141-06

53. Lu J-R, Lu W-W, Lai J-Z, Tsai F-L, Wu S-H, Lin C-W, et al. Calcium flux and calpain-mediated activation of the apoptosis-inducing factor contribute to enterovirus 71-induced apoptosis. J Gen Virol. Society for General Microbiology; 2013; 94: 1477–1485. doi: 10.1099/vir.0.047753-0

54. Broz P, Ruby T, Belhocine K, Bouley DM, Kayagaki N, Dixit VM, et al. Caspase-11 increases susceptibility to Salmonella infection in the absence of caspase-1. Nature. 2012; 490: 288–291. doi: 10.1038/nature11419 PMID: 22895188

55. Aachoui Y, Leaf IA, Hagar JA, Fontana MF, Campos CG, Zak DE, et al. Caspase-11 protects against bacteria that escape the vacuole. Science. 2013; 339: 975–978. doi: 10.1126/science.1230751 PMID: 23348507

56. Wong K-W, Jacobs WR. Critical role for NLRP3 in necrotic death triggered by Mycobacterium tuberculosis. Cell Microbiol. 2011; 13: 1371–1384. doi: 10.1111/j.1462-5822.2011.01625.x PMID: 21740493

57. Willingham SB, Bergstralh DT, O'Connor W, Morrison AC, Taxman DJ, Duncan JA, et al. Microbial pathogen-induced necrotic cell death mediated by the inflammasome components CIAS1/cryopyrin/NLRP3 and ASC. Cell Host and Microbe. 2007; 2: 147–159. doi: 10.1016/j.chom.2007.07.009 PMID: 18005730

58. Aits S, Jäättelä M. Lysosomal cell death at a glance. J Cell Sci. 2013; 126: 1905–1912. doi: 10.1242/jcs.091181 PMID: 23720375

59. Repnik U, Česen MH, Turk B. The endolysosomal system in cell death and survival. Cold Spring Harbor Perspectives in Biology. Cold Spring Harbor Lab; 2013; 5: a008755. doi: 10.1101/cshperspect.a008755

60. Kågedal K, Zhao M, Svensson I, Brunk UT. Sphingosine-induced apoptosis is dependent on lysosomal proteases. Biochem J. Portland Press Ltd; 2001; 359: 335–343.

61. Lee J, Repasy T, Papavinasasundaram K, Sassetti C, Kornfeld H. Mycobacterium tuberculosis induces an atypical cell death mode to escape from infected macrophages. PLoS ONE. 2011; 6: e18367. doi: 10.1371/journal.pone.0018367 PMID: 21483832

62. Deretic V. Autophagy: an emerging immunological paradigm. J Immunol. American Association of Immunologists; 2012; 189: 15–20. doi: 10.4049/jimmunol.1102108

63. Maiuri MC, Zalckvar E, Kimchi A, Kroemer G. Self-eating and self-killing: crosstalk between autophagy and apoptosis. Nat Rev Mol Cell Biol. Nature Publishing Group; 2007; 8: 741–752. doi: 10.1038/nrm2239

64. Mizushima N, Yoshimori T, Levine B. Methods in mammalian autophagy research. Cell. 2010; 140: 313–326. doi: 10.1016/j.cell.2010.01.028 PMID: 20144757

65. Manzanillo PS, Ayres JS, Watson RO, Collins AC, Souza G, Rae CS, et al. The ubiquitin ligase parkin mediates resistance to intracellular pathogens. Nature. 2013. doi: 10.1038/nature12566

66. Watson RO, Manzanillo PS, Cox JS. Extracellular M. tuberculosis DNA targets bacteria for autophagy by activating the host DNA-sensing pathway. Cell. 2012; 150: 803–815. doi: 10.1016/j.cell.2012.06.040 PMID: 22901810

67. Eng KE, Panas MD, Karlsson Hedestam GB, McInerney GM. A novel quantitative flow cytometry-based assay for autophagy. Autophagy. 2010; 6: 634–641. doi: 10.4161/auto.6.5.12112 PMID: 20458170

68. Abdallah AM, Savage NDL, van Zon M, Wilson L, Vandenbroucke-Grauls CMJE, van der Wel NN, et al. The ESX-5 secretion system of Mycobacterium marinum modulates the macrophage response. J Immunol. 2008; 181: 7166–7175. PMID: 18981138

69. Keller C, Mellouk N, Danckaert A, Simeone R, Brosch R, Enninga J, et al. Single cell measurements of vacuolar rupture caused by intracellular pathogens. J Vis Exp. 2013;: e50116–e50116. doi: 10.3791/50116 PMID: 23792688

70. Yuk J-M, Shin D-M, Lee H-M, Yang C-S, Jin HS, Kim K-K, et al. Vitamin D3 induces autophagy in human monocytes/macrophages via cathelicidin. Cell Host and Microbe. 2009; 6: 231–243. doi: 10.1016/j.chom.2009.08.004 PMID: 19748465

71. Matsuzawa T, Kim B-H, Shenoy AR, Kamitani S, Miyake M, MacMicking JD. IFN-γ elicits macrophage autophagy via the p38 MAPK signaling pathway. J Immunol. American Association of Immunologists; 2012; 189: 813–818. doi: 10.4049/jimmunol.1102041

72. Shin D-M, Jeon B-Y, Lee H-M, Jin HS, Yuk J-M, Song C-H, et al. Mycobacterium tuberculosis eis regulates autophagy, inflammation, and cell death through redox-dependent signaling. PLoS Pathog. 2010; 6: e1001230. doi: 10.1371/journal.ppat.1001230 PMID: 21187903

73. He C, Klionsky DJ. Regulation mechanisms and signaling pathways of autophagy. Annu Rev Genet. Annual Reviews; 2009; 43: 67–93. doi: 10.1146/annurev-genet-102808-114910

74. Wang Richard C W YA ZZ ZX GB GW MR JL B. Akt-Mediated Regulation of Autophagy and Tumorigenesis Through Beclin 1 Phosphorylation. Science (New York, NY). NIH Public Access; 2012; 338: 956. doi: 10.1126/science.1225967

75. Muniz-Feliciano L, Van Grol J, Portillo J-AC, Liew L, Liu B, Carlin CR, et al. Toxoplasma gondii-induced activation of EGFR prevents autophagy protein-mediated killing of the parasite. Denkers EY, editor. PLoS Pathog. Public Library of Science; 2013; 9: e1003809. doi: 10.1371/journal.ppat.1003809

76. Owen KA, Meyer CB, Bouton AH, Casanova JE. Activation of focal adhesion kinase by Salmonella suppresses autophagy via an Akt/mTOR signaling pathway and promotes bacterial survival in macrophages. Deretic V, editor. PLoS Pathog. Public Library of Science; 2014; 10: e1004159. doi: 10.1371/journal.ppat.1004159

77. Jo H, Mondal S, Tan D, Nagata E, Takizawa S, Sharma AK, et al. Small molecule-induced cytosolic activation of protein kinase Akt rescues ischemia-elicited neuronal death. Proceedings of the National Academy of Sciences. 2012; 109: 10581–10586. doi: 10.1073/pnas.1202810109

78. Miller JL, Velmurugan K, Cowan MJ, Briken V. The Type I NADH Dehydrogenase of Mycobacterium tuberculosis Counters Phagosomal NOX2 Activity to Inhibit TNF-α-Mediated Host Cell Apoptosis. Deretic V, editor. 2010; 6: e1000864–2. doi: 10.1371/journal.ppat.1000864

79. Welin A, Lerm M. Inside or outside the phagosome? The controversy of the intracellular localization of Mycobacterium tuberculosis. Tuberculosis (Edinb). 2012; 92: 113–120. doi: 10.1016/j.tube.2011.09.009

80. Russell DG. Mycobacterium tuberculosis and the intimate discourse of a chronic infection. Immunol Rev. Blackwell Publishing Ltd; 2011; 240: 252–268. doi: 10.1111/j.1600-065X.2010.00984.x

81. Creasey EA, Isberg RR. The protein SdhA maintains the integrity of the Legionella-containing vacuole. Proceedings of the National Academy of Sciences. National Acad Sciences; 2012; 109: 3481–3486. doi: 10.1073/pnas.1121286109

82. Ruiz-Albert J, Yu X-J, Beuzón CR, Blakey AN, Galyov EE, Holden DW. Complementary activities of SseJ and SifA regulate dynamics of the Salmonella typhimurium vacuolar membrane. Mol Microbiol. 2002; 44: 645–661. PMID: 11994148

83. Rahman MA, Sobia P, Gupta N, Kaer LV, Das G. Mycobacterium tuberculosis Subverts the TLR-2—MyD88 Pathway to Facilitate Its Translocation into the Cytosol. PLoS ONE. 2014; 9: e86886. doi: 10.1371/journal.pone.0086886 PMID: 24475192

84. Repnik U, Stoka V, Turk V, Turk B. Lysosomes and lysosomal cathepsins in cell death. Biochim Biophys Acta. 2012; 1824: 22–33. doi: 10.1016/j.bbapap.2011.08.016 PMID: 21914490

85. Houben ENG, Korotkov KV, Bitter W. Take five—Type VII secretion systems of Mycobacteria. Biochim Biophys Acta. 2014; 1843: 1707–1716. doi: 10.1016/j.bbamcr.2013.11.003 PMID: 24263244

86. Cadieux N, Parra M, Cohen H, Maric D, Morris SL, Brennan MJ. Induction of cell death after localization to the host cell mitochondria by the Mycobacterium tuberculosis PE_PGRS33 protein. Microbiology. 2011; 157: 793–804. doi: 10.1099/mic.0.041996-0 PMID: 21081760

87. Danilchanka O, Sun J, Pavlenok M, Maueröder C, Speer A, Siroy A, et al. An outer membrane channel protein of Mycobacterium tuberculosis with exotoxin activity. Proceedings of the National Academy of Sciences. National Acad Sciences; 2014; 111: 6750–6755. doi: 10.1073/pnas.1400136111

88. Sun J, Siroy A, Lokareddy RK, Speer A, Doornbos KS, Cingolani G, et al. The tuberculosis necrotizing toxin kills macrophages by hydrolyzing NAD. Nat Struct Mol Biol. 2015; 22: 672–678. doi: 10.1038/nsmb.3064 PMID: 26237511

89. Green DR, Levine B. To be or not to be? How selective autophagy and cell death govern cell fate. Cell. 2014; 157: 65–75. doi: 10.1016/j.cell.2014.02.049 PMID: 24679527

90. Galluzzi L, Pietrocola F, Levine B, Kroemer G. Metabolic control of autophagy. Cell. 2014; 159: 1263–1276. doi: 10.1016/j.cell.2014.11.006 PMID: 25480292

91. Deretic V, Saitoh T, Akira S. Autophagy in infection, inflammation and immunity. Nat Rev Immunol. 2013; 13: 722–737. doi: 10.1038/nri3532 PMID: 24064518

92. Gutierrez MG, Master SS, Singh SB, Taylor GA, Colombo MI, Deretic V. Autophagy is a defense mechanism inhibiting BCG and Mycobacterium tuberculosis survival in infected macrophages. Cell. 2004; 119: 753–766. doi: 10.1016/j.cell.2004.11.038 PMID: 15607973

93. Castillo EF, Dekonenko A, Arko-Mensah J, Mandell MA, Dupont N, Jiang S, et al. Autophagy protects against active tuberculosis by suppressing bacterial burden and inflammation. Proceedings of the National Academy of Sciences. National Acad Sciences; 2012; 109: E3168–76. doi: 10.1073/pnas.1210500109

94. Huang D, Bao L. Mycobacterium tuberculosis EspB protein suppresses interferon-γ-induced autophagy in murine macrophages. Journal of Microbiology, Immunology and Infection. Elsevier; 2014;0. doi: 10.1016/j.jmii.2014.11.008

95. Seto S, Tsujimura K, Koide Y. Coronin-1a inhibits autophagosome formation around Mycobacterium tuberculosis-containing phagosomes and assists mycobacterial survival in macrophages. Cell Microbiol. 2012; 14: 710–727. doi: 10.1111/j.1462-5822.2012.01754.x PMID: 22256790

96. Romagnoli A, Etna MP, Giacomini E, Pardini M, Remoli ME, Corazzari M, et al. ESX-1 dependent impairment of autophagic flux by Mycobacterium tuberculosis in human dendritic cells. Autophagy. 2012; 8: 1357–1370. doi: 10.4161/auto.20881 PMID: 22885411

97. Randow F, Youle RJ. Self and Nonself: How Autophagy Targets Mitochondria and Bacteria. Cell Host and Microbe. Elsevier; 2014; 15: 403–411. doi: 10.1016/j.chom.2014.03.012

98. Hou W, Zhang Q, Yan Z, Chen R, Zeh Iii HJ, Kang R, et al. Strange attractors: DAMPs and autophagy link tumor cell death and immunity. Cell Death Dis. 2013; 4: e966. doi: 10.1038/cddis.2013.493 PMID: 24336086

99. Deretic V. Autophagy in Tuberculosis. Cold Spring Harb Perspect Med. Cold Spring Harbor Laboratory Press; 2014; 4: a018481–a018481. doi: 10.1101/cshperspect.a018481

100. Srinivasan L, Ahlbrand S, Briken V. Interaction of Mycobacterium tuberculosis with host cell death pathways. Cold Spring Harb Perspect Med. Cold Spring Harbor Laboratory Press; 2014; 4: a022459–a022459. doi: 10.1101/cshperspect.a022459

101. Bokum ten AMC, Movahedzadeh F, Frita R, Bancroft GJ, Stoker NG. The case for hypervirulence through gene deletion in Mycobacterium tuberculosis. Trends in microbiology. 2008; 16: 436–441. doi: 10.1016/j.tim.2008.06.003 PMID: 18701293

102. Manca C, Tsenova L, Freeman S, Barczak AK, Tovey M, Murray PJ, et al. Hypervirulent M. tuberculosis W/Beijing strains upregulate type I IFNs and increase expression of negative regulators of the Jak-Stat pathway. J Interferon Cytokine Res. 2005; 25: 694–701. doi: 10.1089/jir.2005.25.694 PMID: 16318583

103. Shimono N, Morici L, Casali N, Cantrell S, Sidders B, Ehrt S, et al. Hypervirulent mutant of Mycobacterium tuberculosis resulting from disruption of the mce1 operon. Proc Natl Acad Sci USA. National Acad Sciences; 2003; 100: 15918–15923. doi: 10.1073/pnas.2433882100

104. Parish T, Smith DA, Kendall S, Casali N, Bancroft GJ, Stoker NG. Deletion of two-component regulatory systems increases the virulence of Mycobacterium tuberculosis. Infection and Immunity. 2003; 71: 1134–1140. PMID: 12595424

105. Papavinasasundaram KG, Chan B, Chung J-H, Colston MJ, Davis EO, Av-Gay Y. Deletion of the Mycobacterium tuberculosis pknH gene confers a higher bacillary load during the chronic phase of infection in BALB/c mice. Journal of Bacteriology. American Society for Microbiology; 2005; 187: 5751–5760. doi: 10.1128/JB.187.16.5751-5760.2005

106. Kumar D, Palaniyandi K, Challu VK, Kumar P, Narayanan S. PknE, a serine/threonine protein kinase from Mycobacterium tuberculosis has a role in adaptive responses. Arch Microbiol. 2013; 195: 75–80. doi: 10.1007/s00203-012-0848-4 PMID: 23108860

107. Gopalaswamy R, Narayanan S, Chen B, Jacobs WR, Av-Gay Y. The serine/threonine protein kinase PknI controls the growth of Mycobacterium tuberculosis upon infection. FEMS Microbiol Lett. The Oxford University Press; 2009; 295: 23–29. doi: 10.1111/j.1574-6968.2009.01570.x

108. Foreman-Wykert AK, Miller JF. Hypervirulence and pathogen fitness. Trends in microbiology. 2003; 11: 105–108. PMID: 12648937

109. Galagan JE. Genomic insights into tuberculosis. Nat Rev Genet. Nature Publishing Group; 2014; 15: 307–320. doi: 10.1038/nrg3664

110. Blaser MJ, Kirschner D. The equilibria that allow bacterial persistence in human hosts. Nature. Nature Publishing Group; 2007; 449: 843–849. doi: 10.1038/nature06198

111. Bardarov S, Bardarov SJ Jr, Pavelka MSJ Jr, Sambandamurthy V, Larsen M, Tufariello J, et al. Specialized transduction: an efficient method for generating marked and unmarked targeted gene disruptions in Mycobacterium tuberculosis, M. bovis BCG and M. smegmatis. Microbiology. 2002; 148: 3007–3017. PMID: 12368434

112. Klinkenberg LG, Karakousis PC. Rv1894c is a novel hypoxia-induced nitronate monooxygenase required for Mycobacterium tuberculosis virulence. Journal of Infectious Diseases. Oxford University Press; 2013; 207: 1525–1534. doi: 10.1093/infdis/jit049

113. Skwor TA, Cho H, Cassidy C, Yoshimura T, McMurray DN. Recombinant guinea pig CCL5 (RANTES) differentially modulates cytokine production in alveolar and peritoneal macrophages. J Leukoc Biol. Society for Leukocyte Biology; 2004; 76: 1229–1239. doi: 10.1189/jlb.0704414

114. Flores AR, Parsons LM, Pavelka MS. Genetic analysis of the beta-lactamases of Mycobacterium tuberculosis and Mycobacterium smegmatis and susceptibility to beta-lactam antibiotics. Microbiology (Reading, Engl). Microbiology Society; 2005; 151: 521–532. doi: 10.1099/mic.0.27629-0